Fracture characteristics in Cretaceous platform and overlying ramp carbonates: An outcrop study from Maiella Mountain (central Italy)

Marine and Petroleum Geology xxx (2016) xxx-xxx

Contents lists available at ScienceDirect

Marine and Petroleum Geology

journal homepage: www.elsevier.com

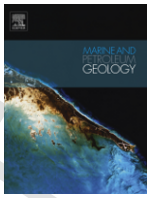

Research paper

Fracture characteristics in Cretaceous platform and overlying ramp carbonates: An outcrop study from Maiella Mountain (central Italy)

Andrea Rustichelli,[a, *] Stefano Torrieri,[a, b] Emanuele Tondi,[a] Salvatore Laurita,[c] Christoph Strauss,[d] Fabrizio Agosta,[c] Fabrizio Balsamo [e]

[a] Geology Division, School of Science and Technology, University of Camerino, Italy
[b] Shell Italia Exploration & Production, Rome, Italy
[c] Department of Sciences, University of Basilicata, Italy
[d] Shell Ukraine Exploration & Production, Kiev, Ukraine
[e] Department of Earth Science, University of Parma, Italy

ARTICLE INFO

Article history:
Received 22 February 2016
Received in revised form 6 April 2016
Accepted 16 May 2016
Available online xxx

Keywords:
Fault damage zone
Vertically persistent fracture
Fracture stratigraphy
Fluid flow
Hydrocarbons

ABSTRACT

This article focuses on field- and laboratory-based characterization of vertically persistent fractures that are part of oblique-slip normal fault zones and crosscut the Cretaceous platform and overlaying ramp carbonates outcropping at Maiella Mountain (central Italy). The achieved results show that: (i) fault damage zones are wider and more densely fractured in the platform carbonates than in the ramp ones; (ii) joints and sheared joints composing the fault damage zones are taller, better connected and less spaced within the former rocks than in the ramp carbonates. The aforementioned structural differences are interpreted to be a consequence of the different mechanical properties of the platform and ramp carbonates during failure. At Maiella Mountain, platform carbonates are, indeed, made up of overall stiffer (higher Uniaxial Compressive Strength values) and less porous rocks, due to more abundant intergranular void-filling cement and presence of matrix.

In terms of hydrocarbon flow and recovery, geometric and dimensional attributes of fractures suggest that the well-connected network of closely spaced fractures cutting across the platform carbonates may form efficient pathways for both vertical and horizontal hydrocarbon flow. In contrast, the relatively poorly connected and low-density fracture network affecting the ramp carbonates is likely less efficient in providing fairways for flowing hydrocarbons.

1. Introduction

Fractures, meant as a collective term encompassing joints, sheared joints and faults, represent the product of brittle deformation due to stress exceeding the intrinsic rock strength and/or the frictional strength. They occur at different scales and can form isolated features as well as be connected to others forming fracture networks (e.g., Watterson, 1986; Pollard and Aydin, 1988). In addition to the intrinsic rock strength and the fracture frictional strength, height and spacing of fractures and the overall fracture distribution within the rock mass can be controlled by mechanically significant interfaces (commonly sedimentary bed surfaces) that may arrest fracture propagation in different ways (Hooker et al., 2013; Fig. 1). The individual rock layers bounded by such interfaces and normally corresponding to single beds or individual bed packages that are characterized by quite homogeneous fracture distribution, due to homogeneous mechanical properties during failure, are named "fracture units" in the terminology of Laubach et al. (2009; Fig. 1).

As documented in literature (e.g., Aydin, 2000; Laubach, 2003; Graham-Wall et al., 2006; Agosta et al., 2010; Solano et al., 2011), fracture networks often represent first-order subsurface pathways for flow of hydrocarbons and other types of geofluids (e.g., groundwater, geothermal and hydrothermal brines). In tight, layered carbonate rocks, this is especially true for fractures characterized by a high vertical persistence (generally taller than 2 m) and commonly crosscutting multiple rock layers (Panza et al., 2015). Based on outcrop measurements and Discrete Fracture Network (DFN) modelling, these authors found that, despite such throughgoing, vertically persistent fractures (VPF) are generally less numerous than fractures confined within individual beds (stratabound fractures; Odling et al., 1999), they account for almost all the overall vertical permeability of the rock due to their greater height and aperture values. For this reason, a comprehensive understanding of geometry, dimensional parameters, connectivity and overall distribution (defining fracture units and interfaces at different scales) of VPF is of paramount importance with regard to subsurface reservoir development and planning recovery of hydrocarbons in carbonates (Garland et al., 2012).

This contribution focuses on the characterization of the VPF networks affecting Bahamian-type inner platform carbonates (Cima delle Murelle Formation; Vecsei, 1991) and overlaying proximal ramp carbonates (Orfento Formation; Crescenti et al., 1969), both Cretaceous in age, which are exposed near the top of Maiella Mountain (central Italy). Accumulating within environments protected from sea waves

* Corresponding author.
Email address: andrea.rustichelli@unicam.it (A. Rustichelli)

http://dx.doi.org/10.1016/j.marpetgeo.2016.05.020
0264-8172/

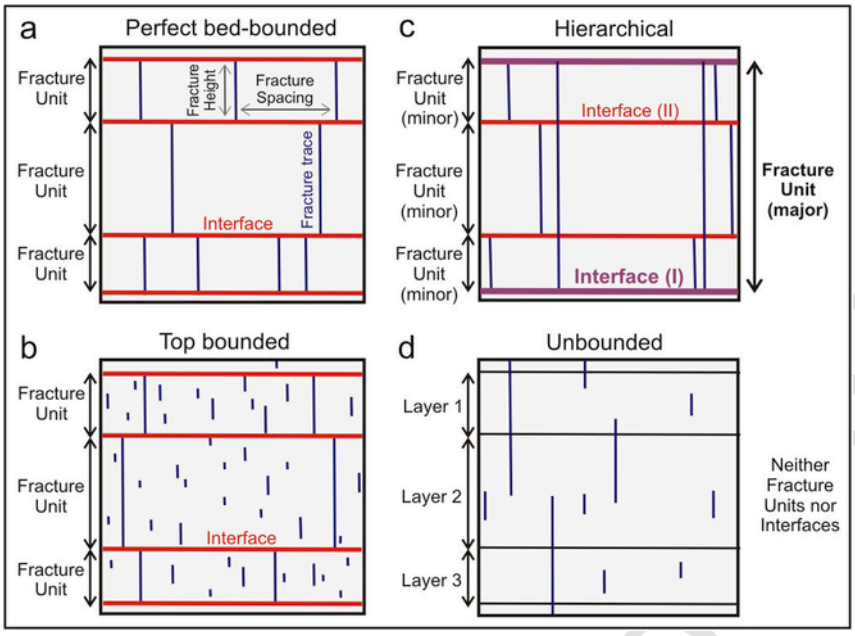

Fig. 1. Cross-sectional views of fractured multilayer media displaying the four (a–d) ideal fracture patterns defined by Hooker et al. (2013) in relation to varying fracture layer boundedness. The concepts of fracture unit and interface (fracture unit boundary), also hierarchical (c), are illustrated. Interface hierarchy in (c): I = first-order; II = second-order.

and normally characterized by low-energy hydrodynamic conditions, such inner platform carbonates are generally fine-grained and less porous than proximal ramp carbonates, which normally accumulate under higher-energy conditions (Eberli et al., 1993; Mutti et al., 1996; Vecsei et al., 1998). As a consequence, the different properties of carbonates formed in these two common depositional settings may have a remarkable impact on characteristics of fractures that develop within them, and therefore on their efficiency in driving fluid flow. In addition, the ramp over platform carbonates stratigraphic configuration might draw the interest of the hydrocarbon industry because VPF may form efficient pathways for hydrocarbon flow (i) from source rocks, commonly present within restricted internal settings of carbonate platforms, (ii) to carbonate reservoirs, which may have large extents where represented by both porous and permeable carbonate bodies accumulated along high-energy proximal settings of carbonate ramps, (iii) throughout (mainly) non-porous platform carbonate strata generally present in between (Tucker and Wright, 1990; Chilingarian et al., 1996).

For instance, this is the case of some onshore oil fields in southern Italy, of which Maiella Mountain is considered a good outcropping analog for fracture characterization (Di Cuia et al., 2009; Masini et al., 2011 and references therein), as it is made of similar fractured carbonate sequences in a comparable structural setting (kilometer-scale thrust-soled anticline). Although, due to differences in terms of burial history and actual pressure regimes experienced by rocks in outcrop and those in the subsurface, some fracture patterns in outcrop may be only partly representative of the subsurface (Laubach et al., 2009; English, 2012), observations made in the Maiella outcrops may be extrapolated and used, with good reliability, in subsurface reservoir models. By means of wellbore analysis, it is possible to pick fracture units and interfaces in the reservoir and consequently, generate fracture layering models. This implementation can indeed be a powerful tool to both predict the main hydrocarbon paths and explain occurrence of rock volumes across the field with different depletion/productivity indexes.

2. Geologic and structural setting

Maiella Mountain is an east-verging, thrust-soled anticline located in the external zone of the central Apennines fold-and-thrust belt (Fig. 2a–b). The Maiella anticline formed between Early and Late Pliocene (e.g., Ghisetti and Vezzani, 2002; Scisciani et al., 2002) and is made up of a ~2 km thick carbonate succession spanning in age from Upper Jurassic to Miocene, and accumulated within different marine settings such as platform, slope, basin and ramp (Vecsei et al., 1998). In addition to reverse and strike-slip faults and minor folds, structural features affecting the Maiella anticline mainly consist of (oblique-slip) normal faults with throws <200 m, resulting from five distinct deformation phases: (i) Cretaceous tectonics (Accarie et al., 1986; Casabianca et al., 2002; Di Cuia et al., 2009); (ii) Miocene-Early Pliocene flexural extension of the foredeep preceding Maiella anticline development (Scisciani et al., 2002); (iii) flexural slip associated with the development of the Maiella anticline (Graham-Wall et al., 2003; Marchegiani et al., 2006; Tondi et al., 2006; Antonellini et al., 2008; Agosta et al., 2009; Aydin et al., 2010); (iv) Quaternary collapse of the overthickened thrust wedge (Ghisetti and Vezzani, 2002); (v) Late Pleistocene – Holocene active tectonics recorded in south Maiella (Pizzi et al., 2010). The western flank (backlimb) of the Maiella anticline is crosscut entirely by a major, high-angle normal fault named Caramanico fault. This westward dipping fault strikes N-S to NNW-SSE, has a maximum throw in excess of 4 km and a fault trace approximately 30 km long. The timing of activity of the Caramanico fault has been disputed in literature: Miocene-Early Pliocene by Scisciani et al. (2002), Quaternary by Ghisetti and Vezzani (2002) and pre-Quaternary by Pizzi et al. (2010).

The study area is the Rava del Ferro gorge, which is located along the western flank of the Maiella anticline (Fig. 2a). Along this gorge, Cretaceous to Paleogene platform and ramp carbonates of the Morrone di Pacentro, Cima delle Murelle, Orfento and Santo Spirito formations crop out extensively (Fig. 2c). These carbonates are extensively fractured and crosscut by small oblique-slip normal faults.

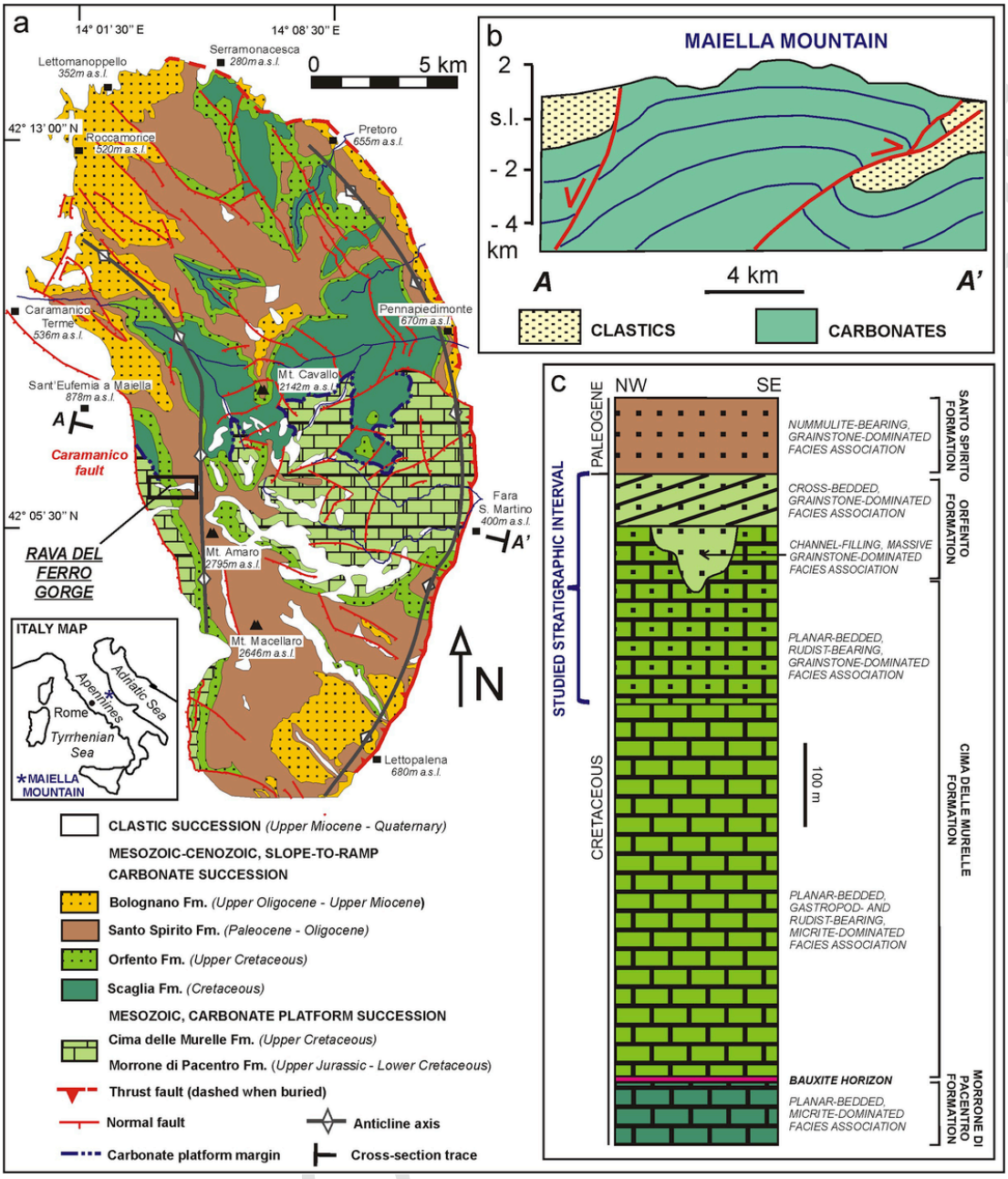

Fig. 2. Location map and geologic framework of Maiella Mountain and the study area. (a) Geologic map of Maiella Mountain (modified after Ghisetti and Vezzani, 2002). (b) Geologic cross-section (modified after Scisciani et al., 2002). (c) Stratigraphic scheme of the carbonate stratigraphic units exposed at the Rava del Ferro gorge.

3. Materials and methods

Data presented in this contribution were gathered by means of field and laboratory analyses.

The field work was carried out along the sub-vertical walls of the Rava del Ferro gorge, at altitudes between 2100 and 2400 m a.s.l. (Figs. 2a and 3). The studied outcrops expose the uppermost strata of the Cima delle Murelle Formation and the entire Orfento Formation (Fig. 2c). The most relevant sites (named A-N in Fig. 3) were selected for detailed stratigraphic, sedimentologic and structural analyses. Typically, these outcrops are tens of meters long and high, and are variably oriented (Fig. 4).

Stratigraphic logs and measurement of parameters such as attitude, thickness and lateral extent of beds were carried out along the aforementioned outcrops to decipher the depositional architecture and sedimentologic features of the studied carbonates. We also performed (i) Schmidt Hammer testing to estimate the present-day Uniaxial Compressive Strength (UCS) of the carbonates, (ii) collection of 20 oriented hand specimens for petrographic studies and porosity measurements, (iii) quantitative structural analysis accomplished by scan lines (1-dimensional lines of observation).

Proceq L/LR-type Schmidt Hammer testing was performed on 16 distinct carbonate layers by considering the following requirements: (i) representativeness of the studied facies, and (ii) distance from depositional and structural discontinuities. The Schmidt Hammer mea-

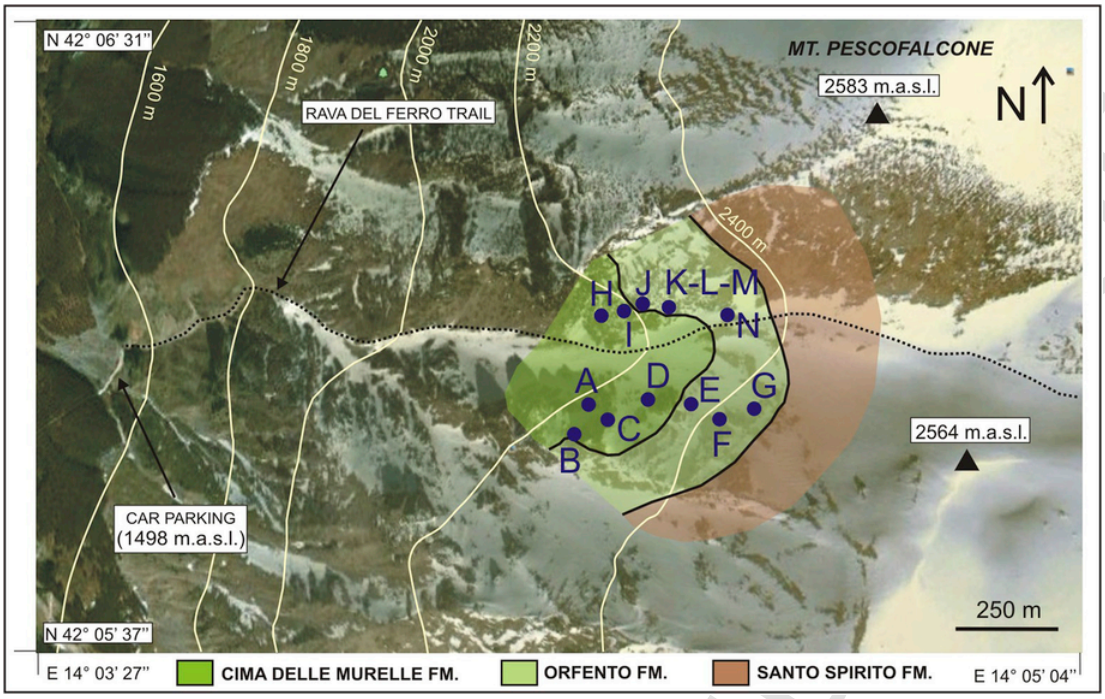

Fig. 3. Aerial plan view from Google Earth of the Rava del Ferro gorge with locations of the surveyed sites (labeled A – N), and distribution of the Cima delle Murelle and Orfento formations in the study area.

sures the number of rebounds of a spring-loaded mass impacting against the surface of the rock. According to the Proceq standard procedure, the number of rebounds was measured 20 times in correspondence to a unique site for each individual layer, holding the hammer orthogonal to flat and smooth, vertical rock surfaces. The 20 rebound number values were subsequently computed by discarding the highest 5 values and lowest 5 ones, hence averaging the 10 remaining values. The mean value of number of rebounds for each layer was thus converted in UCS values by referencing the conversion chart provided by Proceq (Table 1).

Concerning scan lines, each one was oriented horizontally within an individual fracture unit and roughly perpendicular to the most abundant set of VPF affecting the surveyed outcrop. Attitude (strike, dip direction and dip angle), type, spacing, height and aperture of the intersected VPF (at least 2 m high, visible from a distance of approximately 4 m from the outcrop, and generally cutting across more beds) were measured. The Terzaghi (1965) trigonometric correction of fracture spacing values was applied to remove the fracture orientation bias. A total of 12 fracture units were surveyed using this procedure in the field; 7 additional synthetic scan lines were computed by digital image analysis of outcrop photos (Table 2), a procedure already and similarly used by Jacquemyn et al. (2012) in virtually inaccessible outcrops. On the photos, all visible VPF and fault planes, as well as bedding surfaces, were traced in a standard drawing program (CorelDraw). Synthetic scan line analysis provided apparent attitudes of fractures, which could be corrected by comparison with fracture orientation data measured at the base of the outcrops. As photos were taken from a distance greater than 4 m from the outcrop, fracture spacing values are likely overestimated relative to those collected in the field. However, this auxiliary procedure was necessary due to the paucity of accessible outcrops, and nevertheless useful to evaluate spacing between fault planes.

In addition to the computation of synthetic scan lines, digital image analysis of inaccessible outcrops was also used to estimate the Fracture Termination Index (FTI) of the fracture unit interfaces. FTI quantifies the effectiveness of interfaces in stopping fractures and is defined, in percentage, as the ratio between (i) the number of VPF terminating against a given interface separating two fracture units, and (ii) the total number of VPF occurring within both the fracture units and terminating against or passing through the same interface.

Aimed at quantify the regularity of fracture spacing, the coefficient of variation (Cv) of the fracture spacing dataset provided by each scan line is computed (Table 2). Cv is the standard deviation of a given fracture spacing dataset divided by the arithmetic mean (Gillespie et al., 1993). The greater the value of Cv, the more irregular the fracture spacing.

The laboratory work included petrographic analysis of 20 thin sections obtained from the collected hand specimens. Petrographic analysis was carried out using a polarized light microscope (Nikon Eclipse E600 Pol) to study both depositional (grains and matrix) and diagenetic rock components (e.g., cements, dissolution features), as well as the overall rock textures and pore types (*sensu* Choquette and Pray, 1970; Lucia, 1999). The results were used to classify the carbonate rocks according to Dunham (1962) and Embry and Klovan (1971) and, above all, to document the possible lithologic controls on fracture characteristics. A total of 60 photomicrographs (3 for each thin section) were later studied, using the software Image-J 1.32, to quantify the petrographic parameters (i.e., grain size, % components of the rock, (2D) visual porosity) of the carbonate rocks. In particular, the grain size of the rock represents the mean value of the grain diameters measured on thin section photomicrographs, assuming that the individual grains have circular shapes. Both percentage amounts of the rock components (i.e., grains, matrix, cements) and of visual porosity (pores resolvable in thin section, >20 μm in size), were calculated by automatic point counting based on recognition of chromatic differences on thin section photomicrographs. In contrast, the (3D) connected porosity was measured on 20 rock samples via automated mercury porosimeter PoreMaster 33 (Quantachrome Instru-

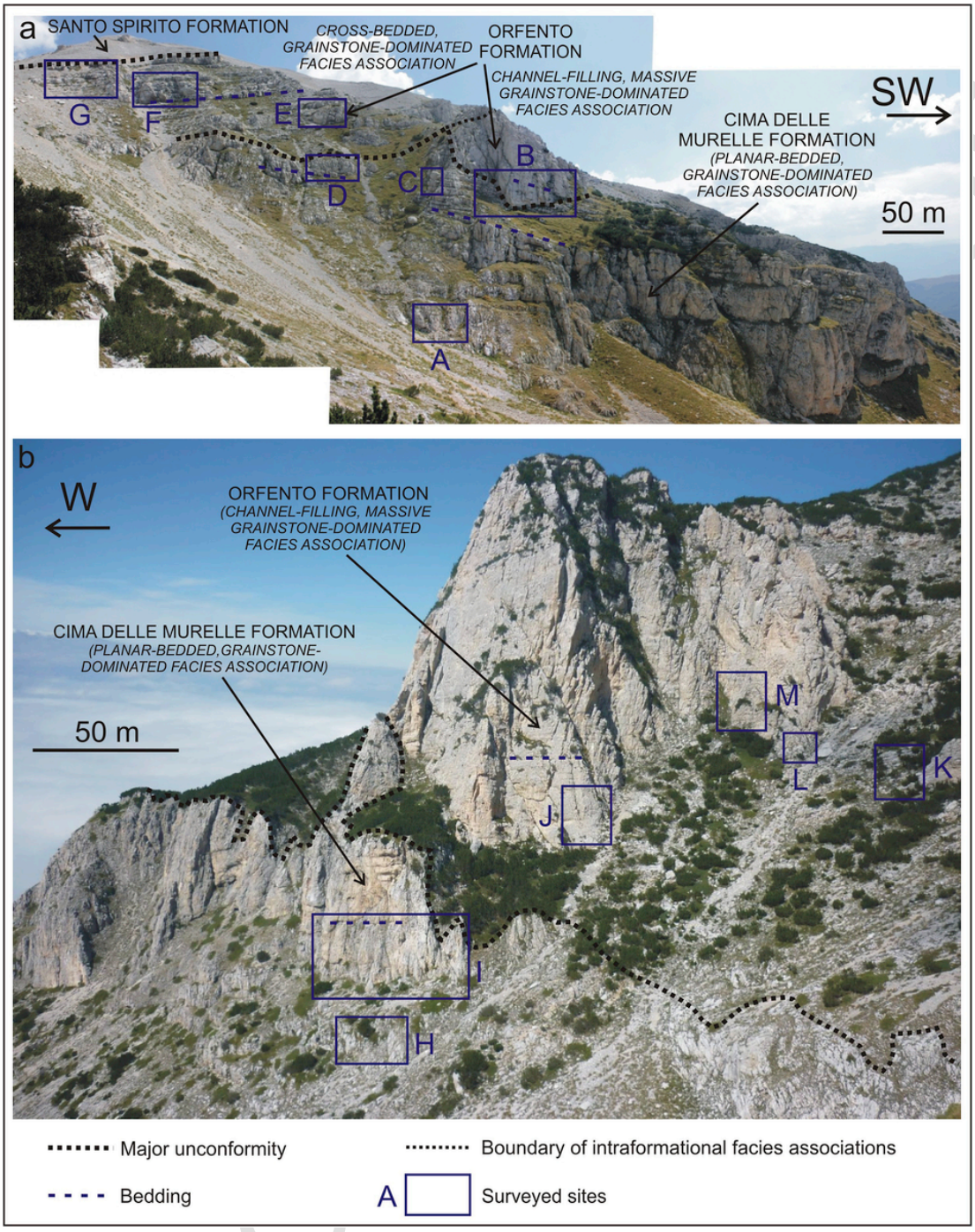

Fig. 4. Panoramic view of the southern (a) and northern (b) walls of the Rava del Ferro gorge, both displaying the unconformable boundary between the Cima delle Murelle and Orfento formations and their facies associations.

ments) at the Department of Earth Science of the University of Parma (Italy).

4. Sedimentologic, petrographic and porosity analyses

Based upon diagnostic characteristics such as depositional architectures, dominant lithologies and biota in skeletal grain assemblages, both Cima delle Murelle and Orfento formations have been subdivided into two facies associations (Fig. 2c). Each facies association is related to a specific depositional environment and includes multiple facies that are distinguishable from each other based upon their differences in rock texture, dominant grain size, sedimentary and biogenic structures, and skeletal assemblages.

The boundary between the Cima delle Murelle and Orfento formations, which is commonly marked (covered) by a narrow vegetated area, is a very gentle angular unconformity characterized by numerous erosional scours (Figs. 4a–b and 5a–b). These U- and V-shaped scours are interpreted as paleochannels (Fig. 4a) and paleogullies (Fig.

Table 1
Mean values of Uniaxial Compressive Strength (UCS), grain size, visual and connected porosity of the studied carbonate facies.

Site code	Formation (facies association)	Facies	UCS (Mpa) (rebound number)	Sample code	Grain size (mm)[a]	Visual porosity (%)	Connected porosity (%)
A	Cima delle Murelle (grainstone-dominated)	Floatstones	80.5 (54.8)	CM1		0.3	0.5
B	Cima delle Murelle (grainstone-dominated)	Packstones	76.8 (52.4)	CM2		2.3	2.7
B	Orfento (massive)	Grainstones		ORF(m)1	00:17	5.5	2.4
B	Orfento (massive)	Grainstones (base-of-channel)	63.5 (46)	ORF(m)2	00:46	11.6	2.9
C	Cima delle Murelle (grainstone-dominated)	Grainstones/Packstones	65 (46.6)	CM3	00:24	2.8	3.6
C	Cima delle Murelle (grainstone-dominated)	Grainstones		CM4	00:13	1.4	8.3
D	Cima delle Murelle (grainstone-dominated)	Grainstones	71.5 (50.2)				
E	Orfento (cross-bedded)	Grainstones		ORF(cb)1	00:19	2.7	4.7
F	Orfento (cross-bedded)	Grainstones	67 (47.6)	ORF(cb)2	00:15	22.4	4.6
G	Orfento (cross-bedded)	Grainstones	67.7 (48.1)	ORF(cb)3	00:16	22.4	6.4
H	Cima delle Murelle (grainstone-dominated)	Grainstones/Floatstones	82 (55.1)	CM5	00:26	2	3.4
I	Cima delle Murelle (grainstone-dominated)	Rudstones	73 (50.7)	CM6		0.5	0.4
I	Cima delle Murelle (grainstone-dominated)	Floatstones	79.5 (53.8)	CM7		2	5.5
I	Cima delle Murelle (grainstone-dominated)	Grainstones	84.5 (56.3)	CM8	00:18	0.2	0.2
J	Orfento (massive)	Grainstones	68.5 (48.8)	ORF(m)3	00:12	8.9	4.8
K	Orfento (massive)	Grainstones		ORF(m)4	00:12	2.2	5.1
L	Orfento (massive)	Grainstones		ORF(m)5	00:24	11	5.4
M	Orfento (massive)	Grainstones	70 (49)	ORF(m)6	00:24	4.3	1.9
N	Orfento (cross-bedded)	Grainstones (thinly cross-bedded)	72.5 (50.2)	ORF(cb)4[b]	00:11	4.2	8
N	Orfento (cross-bedded)	Grainstones (scaly fracturing)	73.5 (50.9)	ORF(cb)5	00:15	11	2
N	Orfento (cross-bedded)	Grainstones (massive bank)	73 (50.5)	ORF(cb)6	00:23	10.6	3.1

[a] Grain size can be calculated only for grainstones. It is not possible to calculate this parameter for the other lithologies because grains are not resolvable in thin section due to smaller (matrix of packstones and floatstones) or larger sizes (floatstones and rudstones).

[b] This sample includes also silt-sized grainstones.

4b), respectively. Both developed during prolonged sub-aerial exposure of the former carbonate platform (Eberli et al., 1993; Mutti et al., 1996; Vecsei et al., 1998).

4.1. Cima delle Murelle Formation

4.1.1. Field observations

The approximately 600 m thick Cima delle Murelle Formation is subdivided into two facies associations (Figs. 2c and 4). The stratigraphically lower facies association, not analyzed in detail in this work, is dominated by whitish to tan micritic limestones arranged in decimeters to meters thick planar beds (Fig. 5c). Collectively, these limestones represent the whole range of Dunham textures: mudstones, wackestones, packstones and grainstones. In contrast, the stratigraphically upper facies association, the focus of this work, is dominated by grainstones and minor packstones arranged in decimeters to a few meters thick planar beds, commonly thinner than in the previous facies association (Figs. 4 and 5). Both grainstones and packstones are from fine-to coarse-grained, whitish, greyish and tan in color, and yielded UCS values ranging between 65 and 84.5 MPa (Table 1). Floatstone and rarer rudstone banks, mostly meters thick (not exceeding 10 m), from tens of meters to approximately 100 m laterally extensive, are intercalated within both facies associations (Fig. 5d). Both floatstones and rudstones are dominated by rudite-sized nerineid gastropods in the lower facies association, and radiolitid rudists in the upper one. Floating rudists, in some cases preserved as molds locally enlarged by karstic dissolution, are typically cm-sized, unfragmented, and have the longitudinal axis parallel to bedding.

4.1.2. Petrographic and porosity features

Only the grainstone-dominated facies association has been petrographically analyzed. Texturally, the sampled rocks consist of bioclastic grainstones and minor packstones, floatstones and rudstones (Fig. 6a–d). All these rocks are mainly composed of rudist fragments, minor benthic foraminifera, and sporadic echinoid plates and spines. Grain sorting varies from very poor to moderate. Clay-to silt-sized calcareous matrix represents up to approximately 25% vol of the whole rock within some floatstones and packstones (Fig. 6c–d). Burrowing is common in grainstones and packstones (Fig. 6d). Cement is dominantly intergranular void-filling (up to 30% vol in facies with minimal or no matrix, such as rudstones and some grainstones and floatstones, Fig. 6a–b), and consists of mosaics of finely sparry to microsparry, equant crystals of clear calcite. Neomorphic cements also occur as replacements of the former aragonitic parts of rudists (Fig. 6a). These cements represent up to over 20% vol of the whole rock and consist of (i) mosaics of coarse sparry, equant and clear calcite crystals; (ii) coarse sparry, bladed, radiaxial calcite crystals; and (iii) very coarse calcite crystals with undulose extinction under cross-polarized light.

Visual porosity ranges from 0.2 to 2.8%, 1.45% on average (Table 1), and is typically patchily distributed. Both pore sizes and geometries vary a lot. Intergranular porosity represents the dominant type, whereas vuggy and moldic porosities are less abundant. Values of

Table 2
Mean values and ranges (±1σ standard deviation) of fracture spacing and height estimated by both true (upper table) and synthetic (lower table) scan lines. Surveyed site codes refer to Fig. 4; Scan line codes refer to Figs. 8–10. * = rudist floatstone banks over 2 m thick.

Surveyed site code	Formation (facies association)	Fracture strike range	Fracture spacing – mean value (cm)	Fracture spacing – standard deviation (cm)	Fracture spacing – coefficient of variation (Cv)
A	Cima delle Murelle (grainstone-dominated)	N150–170	25.2	8.9	0.35
B	Cima delle Murelle (grainstone-dominated)	N60–90	i) 13.7 ii) 22.8	i) 5.9 ii) 16.7	i) 0.43 ii) 0.73
C	Cima delle Murelle (grainstone-dominated)	N45–65	8.9	4.7	0.53
D	Cima delle Murelle (grainstone-dominated)	N150–160	62.1	8.5	0.14
H	Cima delle Murelle (grainstone-dominated)	i) N70 ii) N160–170 iii) N150–180	i) 65.5* ii) 80.2* iii) 28.2*	i) 50.1* ii) 43.9* iii) 12*	i) 0.76* ii) 0.55* iii) 0.43*
I	Cima delle Murelle (grainstone-dominated)	N140–160	i) 9.3 ii) 65.2* iii) 18.3	i) 3.1 ii) 15.4* iii) 7	i) 0.33 ii) 0.24* iii) 0.38
N	Orfento (cross-bedded)	N155–170	48.1	40.3	0.84

Scan line code	Formation (facies association)	Approximate fracture strike	Fracture spacing – mean value (m)	Fracture spacing – standard deviation (m)	Fracture spacing – coefficient of variation (Cv)	Fracture height – mean value (m)	Fracture height – standard deviation (m)
A-A′	Cima delle Murelle (grainstone-dominated)	N160	15.21	9.23	0.61	66.39	42.56
B-B′	Orfento (massive)	N160	10.82	5.03	0.44	32.93	18.49
C-C′	Orfento (cross-bedded)	N160	16.30	14.33	0.88	16.78	21.69
D-D′	Cima delle Murelle (grainstone-dominated)	N160	0.42	0.21	0.5	2.04	0.75
E-E′	Orfento (massive)	N160	0.77	0.60	0.78	2.74	0.81
F-F′	Cima delle Murelle (grainstone-dominated)	N160	4.93	3.15	0.59	43.15	18.47
G-G′	Orfento (massive)	N160	6.02	3.47	0.63	46.85	23.96

connected porosity range from 0.2 to 8.3%, 3.1% on average (Table 1). However, the highest measured values are likely overestimated due to the common occurrence of microcracks (Fig. 6a–b). For this reason, the true values of connected porosity of the unfractured rock ("matrix porosity") probably don't exceed the values of visual porosity.

4.1.3. Depositional environment and diagenetic interpretation

According to previous authors (Eberli et al., 1993; Vecsei et al., 1998), carbonates belonging to the Cima delle Murelle Formation and exposed at the Rava del Ferro gorge can be interpreted as being accumulated on the interior (broad shallow-lagoonal to peritidal settings) of an isolated, flat-topped carbonate platform developed under tropical to sub-tropical climatic conditions ("Bahamian-type carbonate platform"). The micrite-dominated facies association accumulated under dominant low-energy conditions, where tidal currents represented the main hydrodynamic process. In contrast, the grainstone-dominated facies association was deposited under relatively higher-energy conditions, as a consequence of the action of more energetic marine currents and storm events. The relatively great thickness of the rudist floatstone banks suggests that these are likely the result of the most energetic depositional events.

Diagenesis of the carbonates belonging to the Cima delle Murelle Formation is considered similar to that experienced by the Orfento Formation (see the Section 4.2), although the former formation underwent a more pronounced cementation.

4.2. Orfento Formation

4.2.1. Field observations

In the study area, the Orfento Formation is from 70 to 170 m thick. It is mostly made up of fine-to medium-grained grainstones, whitish in color and characterized by UCS values ranging between 63.5 and 73.5 MPa (Table 1). Two facies associations are distinguished (Figs. 2c and 4).

The lower one is a channel-filling massive facies association, up to 100 m thick, which occurs in places at the bottom of the formation. This facies association is mostly made up of grainstones arranged in 20 cm to 2 m thick, crude planar beds (Figs. 4 and 5a), rarely displaying a subtle planar lamination. Rudist-bearing floatstones and rudstones arranged in planar beds up to approximately 1 m thick are rarely intercalated. At the bottom of the large paleochannel, a lens-shaped breccia layer up to approximately 1 m thick is exposed on the southern wall of the Rava del Ferro gorge (Fig. 4a, surveyed site B). These semi-lithified breccias consist of heterometric and angular calcareous lithoclasts, which are sand-to silt-sized and greyish, whitish and tan in color (Fig. 5a). The upper facies association is approximately 70 m thick and cross-bedded. The individual beds are a few tens to hundreds of meters laterally extended, from 5 cm to 4 m thick and originally dipping (<5°) towards the NNW (Figs. 4 and 5e–f). Rare lithoclastic rudstone beds with some meters lateral extent are embedded within the grainstones (Fig. 5f). Both facies associations show common bed amalgamation and presence of 20–60 cm thick grainstone beds showing a pervasive scaly fracturing (Fig. 5a, e).

4.2.2. Petrographic and porosity features

All the analyzed rock samples are bioclastic grainstones, which are composed almost entirely of sub-rounded to sub-angular rudist fragments, rare echinoid plates and spines, sporadic benthic foraminifera (*Orbitoides*) and bivalve fragments. Grainstones are generally sand-sized (Fig. 6e–g) and occasionally silt-sized (Fig. 6h). Sorting is commonly good, matrix is absent. Burrowing is generally ubiquitous, especially in the cross-bedded facies association (Fig. 6g). Cement types are similar to those documented in the Cima delle Murelle For-

Fig. 5. Outcrop views of the Cima delle Murelle and Orfento formations. a) Very gentle angular unconformity separating the channel-filling, massive facies association of the Orfento Formation (**ORF-m**) from the underlying Cima delle Murelle Formation (**CM**). Note the channel-lag, lens-shaped breccia layer (**br**). Surveyed site B (cf. Fig. 3 and 4a). b) Sharp boundary between the cross-bedded facies association of the Orfento Formation (**ORF-cb**) and the underlying Cima delle Murelle Formation (**CM**), characterized by planar beds horizontal at time of deposition. **SS** = Santo Spirito Formation. Surveyed sites D-E (cf. Fig. 3 and 4a). c) Micrite-dominated facies association of the Cima delle Murelle Formation. d) Floatstone bank of the Cima delle Murelle Formation. Note the floating rudists (**r**) with longitudinal axis parallel to bedding. e) Three distinct facies belonging to the cross-bedded facies association of the Orfento Formation (**m** = massive grainstone bed; **cb** = cm-thick, cross-bedded grainstone beds; **sf** = grainstones displaying a pervasive scaly fracturing). Surveyed site N (cf. Fig. 3). f) Lens-shaped rudstone layer (**ru**) embedded within the grainstones of the cross-bedded facies association of the Orfento Formation (surveyed site F, c.f. Fig. 3 and 4a). The 33-cm long hammer is for scale.

mation; only the intergranular void-filling cement is by far less abundant (from <1% to a few units % vol of the whole rock).

Visual porosity values of the Orfento Formation vary, bed-by-bed, from 1.9 to 22.4% (10.2% on average; Table 1). Overall, the cross-bedded facies association is more porous (11.8% of average visual porosity) than the massive one (visual porosity values ranging from 4.3 to 11.6%, 8.3% on average; Table 1). In the sand-sized grainstones of both facies associations, visual porosity is dominantly intergranular; moldic and vuggy porosities are less abundant. Pores are relatively less varying in pore sizes and geometries than in the rocks of the Cima delle Murelle Formation, and are more uniformly distributed in the most porous beds (Fig. 6e–f). In contrast, the sporadic silt-sized grainstones (~2% of visual porosity) are characterized by dominant vuggy and moldic pores. Values of connected porosity in the Orfento Formation range between 1.9 and 8%, 4.3% on average (Table 1), which means that most of the visual porosity is not connected. Because of the absence of microcracks, the measured con-

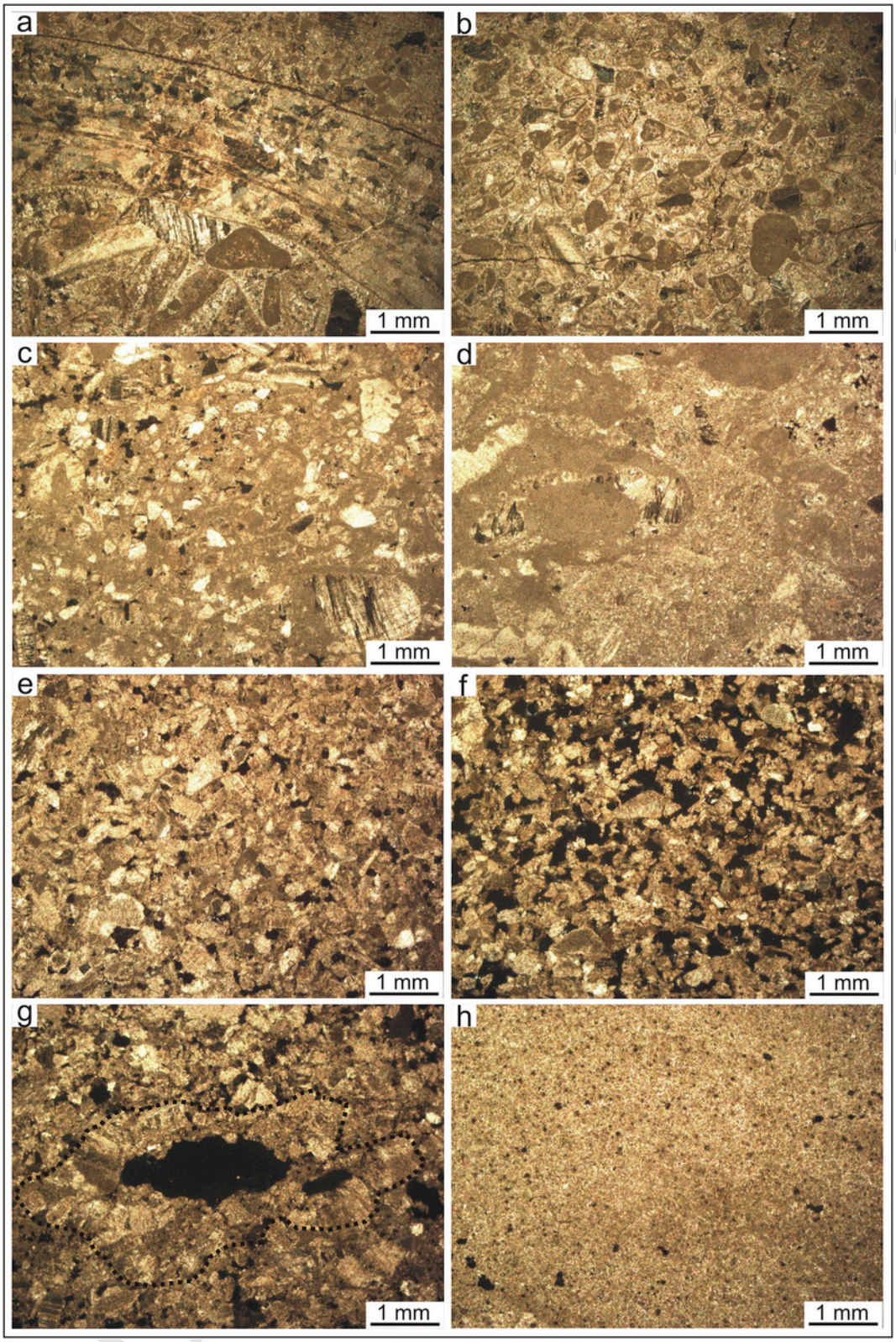

Fig. 6. Microfacies of the Cima delle Murelle (a–d; grainstone-dominated facies association) and Orfento (e–h) formations under cross-polarized light. a) Floatstones including a large rudist fragment composed of neomorphic calcite. b) Grainstones crosscut by joints and calcite veins. c) Packstones. d) Burrowed packstones. e) Low-porosity grainstones of the massive facies association. f) High-porosity grainstones of the cross-bedded facies association. g) Grainstones of the cross-bedded facies association containing burrows (large pores surrounded by rims of compacted grains). h) Silt-sized grainstones of the cross-bedded facies association.

nected porosity values correspond to the amount of connected matrix porosity.

4.2.3. Depositional environment and diagenetic interpretation

As a whole, the carbonates of the Orfento Formation have been interpreted as being accumulated on a distally steepened carbonate ramp, under high-energy hydrodynamic conditions and tropical to sub-tropical climate (Eberli et al., 1993; Mutti et al., 1996; Vecsei et al., 1998). The Orfento Formation carbonates exposed along the Rava del Ferro gorge resemble the facies 4, 5, 6 and 7 of Mutti et al. (1996), and are collectively interpreted as being accumulated in shallow-marine, proximal ramp environments dominated by tidal currents, waves and occasional storms.

Both an earlier aggradational stage and a later progradational stage were documented in the Orfento Formation (Mutti, 1995; Mutti et al., 1996; Vecsei et al., 1998). During the aggradational stage, the intra-platform depressions (channels and gullies) that developed during the long-lasting sub-aerial exposure of the former carbonate platform, were filled by massflow and likely, turbidite deposits (i.e., massive facies association). Subsequently, these deposits and the older platform carbonates (Cima delle Murelle Formation) were topped by bioclastic sand waves (i.e., cross-bedded facies association), which prograded basinward for kilometer distances likely under the influence of tidal currents.

The breccia layer located at the bottom of a large paleochannel (Fig. 4a, surveyed site B) is composed of calcareous lithoclasts likely eroded from the underlying Cima delle Murelle Formation; these breccias may therefore represent a channel lag.

On the basis of cathodoluminescence patterns and stable isotopes, Mutti (1995) interpreted the bulk of calcite cements of the Orfento Formation as precipitated during early meteoric diagenesis consequently to dissolution of former aragonite occurred during short-lived emersion periods of the carbonate ramp. According to the same author, the dissolution of aragonitic grains produced the moldic porosity.

5. Structural analysis

In this section, the results of the structural analysis are first described and then statistically analyzed. Subsequently, they are discussed in terms of genetic mechanisms of fractures and their relation with the structural evolution of Maiella Mountain.

5.1. Structural features

Although unaffected by very large faults and unfolded at the outcrop scale with beds regularly dipping up to 30° to the WNW (Fig. 7), the studied carbonates of the Cima delle Murelle and Orfento formations are affected by numerous fractures with various heights. These can be grouped in two broad categories:

(i) open fractures (seemingly joints; Fig. 5c–f) and minor calcite veins, which are from sub-meter to approximately 2 m high. Fractures and veins are commonly bed-perpendicular and either stratabound or shorter than single bed thickness (perfect bed-bounded to top-bounded fractures *sensu* Hooker et al., 2013; Fig. 1);

(ii) throughgoing fractures with similar attitude of the previous open fractures and veins, but generally higher than 2 m, up to over 100 m (Table 2). These vertically persistent fractures (VPF) encompass joints, sheared joints and fault planes, which cut across bed packages and partly abut against a hierarchy of sedimentary interfaces (hierarchical and top-bounded fractures *sensu* Hooker et al., 2013; Fig. 1).

Considering the purpose of the study, only the VPF are documented and discussed in the next paragraphs and sections.

VPF consist of planar to slightly undulated discontinuities that were commonly enlarged by karstic dissolution and can be infilled with recent soil along erosional recesses (Table 2, Figs. 8–12). Fracture aperture is between <1 mm and 5 cm (2–3 mm on average). The greatest aperture values are mostly due to karstic dissolution. These fractures are interpreted as joints and sheared joints, as they display where relatively unweathered, rare diagnostic plumose structures on their surfaces (Pollard and Aydin, 1988). In addition, sheared joints can display striae on their surfaces, have normal throws <1 cm and attitudes similar to joints, and are characterized by low (<0.01) displacement/length ratios; all typical features of sheared joints (Wilkins et al., 2001).

VPF commonly surround fault planes with normal throws ranging from >1 cm to 25 m, and strike sub-parallel to them (Fig. 7). VPF are therefore part of fault damage zones. Fault cores are associated only with the major fault planes and are <1 m thick. Cores are made up of weakly calcite-cemented fault breccias, which are less resistant to weathering than the surrounding host rock, and hence form negative reliefs often covered by narrow strips of grass (Fig. 11a–b).

Fault damage zones are up to 300 m wide in the Cima delle Murelle Formation (grainstone-dominated facies association), commonly wider at the fault hanging walls (Figs. 8, 10 and 11a–b). The widest damage zones, which also include multiple small faults (Figs. 8 and 10), consist of swarms of fractures several meters to over 100 m high (Table 2), either synthetic or antithetic to the fault planes, and showing numerous lateral and vertical abutting relationships among fractures (well-connected fracture network). Fracture spacing measured in the field varies from 5 cm to 1 m (approximately 40 cm on average; Table 2, Fig. 11d), whilst fracture spacing measured by means of synthetic scan lines on panoramic outcrop pictures (Figs. 8 and 10) is between 1 m and 40 m (Table 2). In all cases, fractures are quite regularly spaced (Cv values range between 0.14 and 0.76; Table 2).

Joints and sheared joints are arranged as two main pairs of sets striking mainly N140-180E and secondly N45-70E, and dipping 65°–90° both NE and SW or NW and SE, respectively (Fig. 7). Fractures of both pairs of sets abut against the fault planes (Figs. 8, 10 and 11a–b). The fault planes appear planar to slightly undulated, and form two main pairs of sets striking N150-170E and N50-65E, respectively, dipping in opposite directions with angles between 60° and 80° (Fig. 7). The two pairs of fault sets and associated VPF show mutual cross-cutting relationships, albeit NNW-SSE striking faults generally dislocate earlier WSW-ENE ones (Fig. 11a). Faults are at least a few hundreds of meters high (corresponding to outcrop dimensions) and mainly show normal throws between several centimeters and tens of centimeters, rarely meters (up to 25 m; Fig. 11a).

Within the Orfento Formation, fault damage zones are more developed within its massive facies association, within which they occur in places (the best exposure is along the northern wall of the surveyed gorge, Figs. 4b and 10). Individual fault damage zones are up to 40 m wide; in some cases, multiple damage zones are overlapped and overall can exceed 100 m in width. Fault zones consist of networks of oblique to vertical fractures from a few meters to over 100 m high, and spaced from 20 cm to 20 m (Table 2, Figs. 8–10). Fractures form two sets striking N160-185E and dipping either E or W with angles ranging between 60° and 85° (Figs. 7 and 10). Among these, only a few fractures dip to the E; all others form individual swarms of

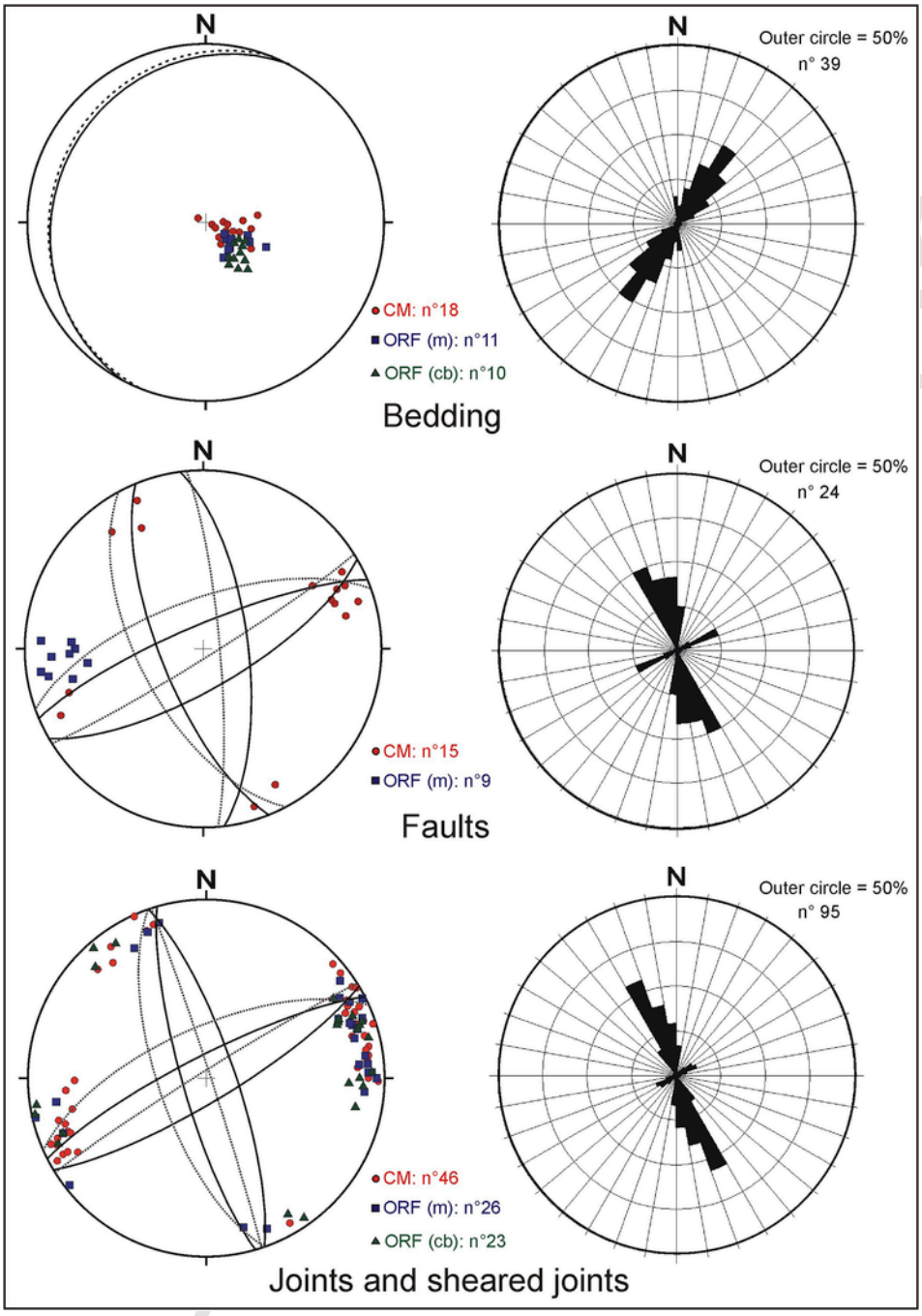

Fig. 7. Stereographic projections (lower hemisphere) of the measured planar structural elements (faults and joints/sheared joints) and bedding of the studied carbonates. On the left, poles of planes (facies associations are distinguished) and mean great circles showing the mean attitude of bedding and joint and fault sets (facies associations are considered as a whole). Dashed mean great circles are referred to either joints/faults restored to unfolded bedding, or bedding without considering the ORF (cb) cross-beds. However, as the two bedding great circles have very similar attitude, cross-beds do not produce a significant bias in restoring joint and fault data. On the right, rose diagrams showing the strike frequencies of the analyzed planar elements. CM = Cima delle Murelle Formation (grainstone-dominated facies association); ORF (m) = Orfento Formation (massive facies association); ORF (cb) = Orfento Formation, (cross-bedded facies association).

shorter fractures that dip to the W and abut against the previous set (Fig. 10), providing good fracture connectivity. The highest E-dipping fractures generally display 1–5 cm normal throws, and are interpreted as incipient faults (Fig. 10). In contrast, all other E- and W-dipping fractures consist of joints and sheared joints occurring within the fault damage zones.

Regarding the cross-bedded facies association of the Orfento Formation, VPF within fault damage zones (<100 m width) are relatively scarce and poorly connected both vertically and laterally. These fractures are arranged in two pairs of sets striking either N150-190E (mostly) or N45-60E and dipping 70°–90° on opposite directions (Fig. 7). VPF attain heights up to 20 m and are generally spaced from 10 cm to approximately 50 m, depending on the observation distance

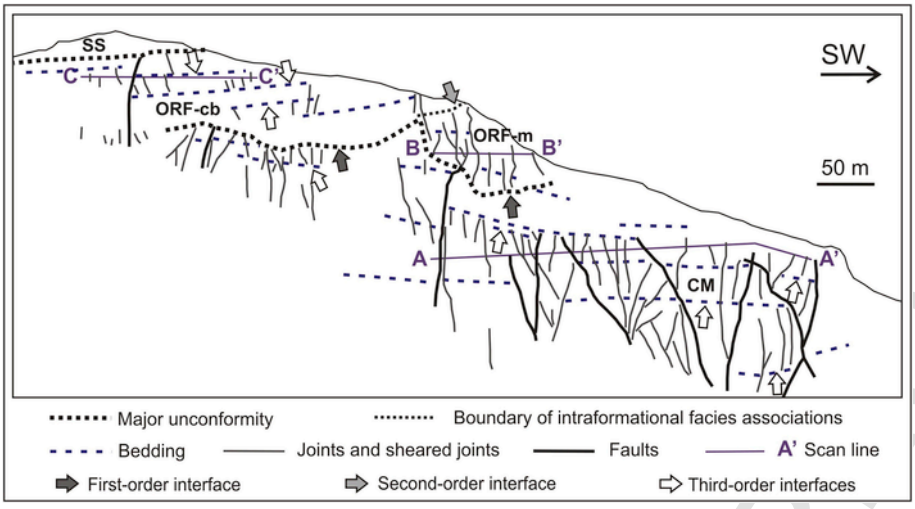

Fig. 8. Cross-sectional drawing from mapping of both stratigraphic and structural elements on the photomosaic of Fig. 4a. Areas lacking such elements are covered by vegetation and recent slope debris. CM = Cima delle Murelle Formation (grainstone-dominated facies association); ORF-m = Orfento Formation (massive facies association); ORF-cb = Orfento Formation, (cross-bedded facies association); SS = Santo Spirito Formation.

(Table 2, Figs. 8, 12b). Fractures are less regularly spaced (Cv varies from 0.84 to 0.88) than in the other facies associations of the Orfento and Cima delle Murelle formations (Cv ≤ 0.78; Table 2).

5.2. Statistical analysis of fracture spacing

Fracture spacing is statistically determined for both formations by coupling field and synthetic scan lines (Table 2). Although mostly reliable, the other measured structural parameters such as fracture height, fracture aperture and fault damage zone width might be partly biased by outcrop dimensions, karstic dissolution and overlap of multiple damage zones, respectively. For these reasons, these parameters are not statistically analyzed.

Fig. 13 displays cumulative frequency distributions of spacing computed for the analyzed fractures: joints (plus sheared joints) and faults. Fault spacing is meant as the horizontal separation between two fault planes. Two different spacing distributions result for each of the three analyzed stratigraphic units (Cima delle Murelle Formation and the two facies associations of the Orfento Formation), which are characterized by different slopes of the best-fit correlation lines, quantitatively expressed by the coefficients of the relative equations ranging between −0.16 and −0.38, and between −1.07 and −1.61, respectively. Spacing distributions with gentler slopes mostly refer to joints characterized by spacing values < 1 m. By contrast, spacing distributions with steeper slopes are mainly related to faults with spacing values > 5 m. A 1–5 m arbitrary threshold between the two aforementioned spacing distributions can be assigned to all three stratigraphic units.

5.3. Structural interpretation

Most of the outcrops are virtually inaccessible as many fracture surfaces have experienced severe surface weathering and dissolution, and fault planes are commonly weathered or covered by grass. Because of this, our field data and observations are tied to relevant literature in order to interpret genetic mechanisms, kinematics and timing of faults and fractures and their relation with the structural evolution of Maiella Mountain.

The documented faults showing normal throws, and the associated VPF are arranged as two approximately orthogonal pairs of sets showing mutual cross-cutting relationships, albeit the dominant NNW-SSE striking faults commonly displace those striking WSW-ENE. Stereoplots of Fig. 7 suggest the occurrence of conjugate pairs of high-angle normal faults and VPF developed after bed tilting. In contrast, field observations reveal that part of faults and VPF likely formed prior to the bed tilting, according to the orthogonal-to-bedding acute bisectors of dihedral angles formed by pairs of fractures (faults and related VPF) with a same strike but opposite dip directions (Figs. 10 and 12a).

Based on good fitting with several structural studies on Maiella Mountain (Marchegiani et al., 2006; Antonellini et al., 2008; Agosta et al., 2009), and the most widely accepted models of faulting related to folding (Stearns, 1968; Price and Cosgrove, 1990), the documented fault zones are considered part of the oblique-slip normal fault systems with similar orientations that have been largely documented in the central and northern Maiella (Fig. 2a). These fault systems have been associated with the development of the Maiella anticline, occurred in Early to Late Pliocene times, and have been interpreted as the product of flexural slip associated with the Maiella folding and thrusting (Graham-Wall et al., 2003; Agosta et al., 2009; Aydin et al., 2010). In this scenario, the dominant NNW-SSE striking faults can be interpreted as oblique-slip normal faults with a minor left-lateral component of motion; whereas the ENE-WSW striking faults are interpreted as oblique-slip normal faults with a more pronounced, right-lateral component of motion (Marchegiani et al., 2006; Antonellini et al., 2008). The mutual cross-cutting relationships between the aforementioned fault sets and associated VPF are consistent with their penecontemporaneous activity, according to the regional paleostress field associated with shortening of the central Apennines, characterized by an E–W oriented maximum horizontal principal stress axis (Bigi et al., 1992). Faults and VPF likely formed during the final stages of the Maiella anticline development, as faults and fractures post-dating folding-related bed tilting (Fig. 7) seem to prevail on pre-tilting structures (Figs. 10 and 12a).

Pre-tilting faults and VPF may also be related to older deformation phases. ~N-S and ~E-W trending, pre-tilting conjugate normal fault systems have been documented by Scisciani et al. (2002) and associated with Miocene-Early Pliocene flexural extension of the foredeep preceding Maiella anticline development. Albeit evidence for syn-sedimentary faults are not found in the studied Cretaceous carbonates,

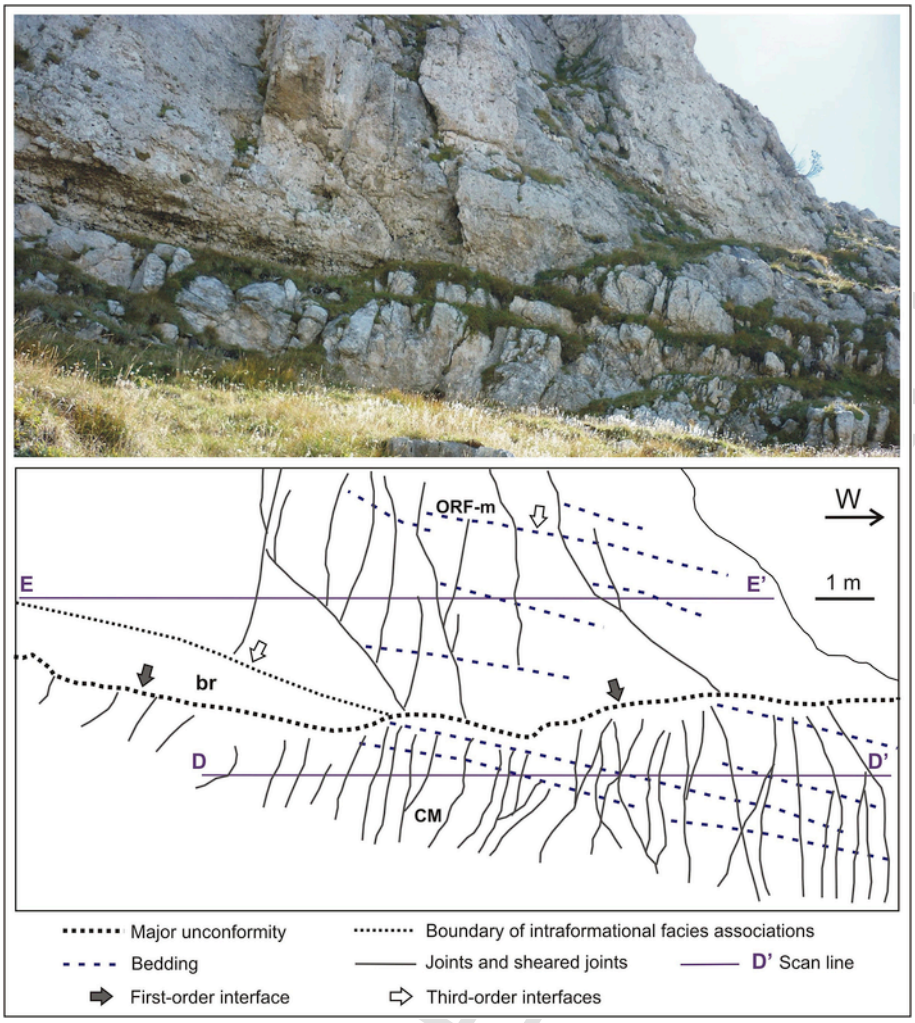

Fig. 9. Cross-sectional drawing from mapping of both stratigraphic and structural elements on a photo of the surveyed site B (cf. Fig. 3 and 4a), showing the boundary between the massive facies association of the Orfento Formation (**ORF-m**) and the underlying grainstone-dominated facies association of the Cima delle Murelle Formation (**CM**). Note the unfractured channel-lag breccia layer (**br**).

NNW-SSE striking Cretaceous normal faults have been documented close to the Maiella platform margin (Accarie et al., 1986; Casabianca et al., 2002; Di Cuia et al., 2009). Heritage of such Cretaceous to Early Pliocene faults during faulting associated with the development of the Maiella anticline is not documented but cannot be excluded.

The NNW-SSE striking, westward-dipping faults and VPF (Fig. 7) that likely formed after bed tilting, may also be the product of Quaternary activity of the Caramanico fault (Ghisetti and Vezzani, 2002), which is located approximately 1–2 km westward of the investigated outcrops. This inference may be supported by the fact that NNW-SSE striking faults commonly displace older WSW-ENE striking faults. However, the damage zone of the Caramanico fault seems to be located downslope (westward) with respect to the studied outcrops, at altitudes between 1500 and 1700 m a.s.l., along the Rava del Ferro gorge (Fig. 3). There, we observed impressive swarms of closely-spaced and steeply inclined VPF, which strike ~N-S and dip westward. Therefore, we exclude that prominent Quaternary faulting affected the studied outcrops, which did not show evidence for Late Pleistocene – Holocene active tectonics documented by Pizzi et al. (2010) in southern Maiella.

As most of the uplift and associated erosion of the Maiella anticline has been ascribed to Quaternary rather than Pliocene folding and thrusting (Ghisetti and Vezzani, 2002), the investigated faults and VPF likely formed at 0.5–1 km burial depths and possibly more. This estimate is based on thickness of the reconstructed Eocene to Lower Pliocene stratigraphic succession that originally overlay the Rava del Ferro Cretaceous carbonates (Vecsei et al., 1998; Ghisetti and Vezzani, 2002). Hence, fault zones similar to those we document can actually be present in buried carbonate successions underlying fold and thrust belts (e.g., onshore oil fields in the southern Italy).

Development of the fault zones in terms of fracturing and faulting mechanisms can be explained integrating our field observations with the existent literature on faulting mechanisms in carbonate multilayers of Maiella Mountain. Fault planes and VPF swarms present in the fault damage zones may be the result of different processes such as:

(i) in-plane propagation throughout multiple beds of earlier open fractures and veins, affecting single beds and reactivated through flexural slip during the Maiella folding (e.g., Graham-Wall et al., 2003; Antonellini et al., 2008; Agosta et al., 2009; Aydin et al., 2010). Similar attitudes of open fractures (seemingly joints) and veins, and VPF support this deformation mechanism, which may have been responsible for the documented normal faulting and normal shearing of fractures (i.e., sheared joints), with formation of new vertically persistent pinnate (horse-tail) joints (Fig. 10) due to either changes of the ap-

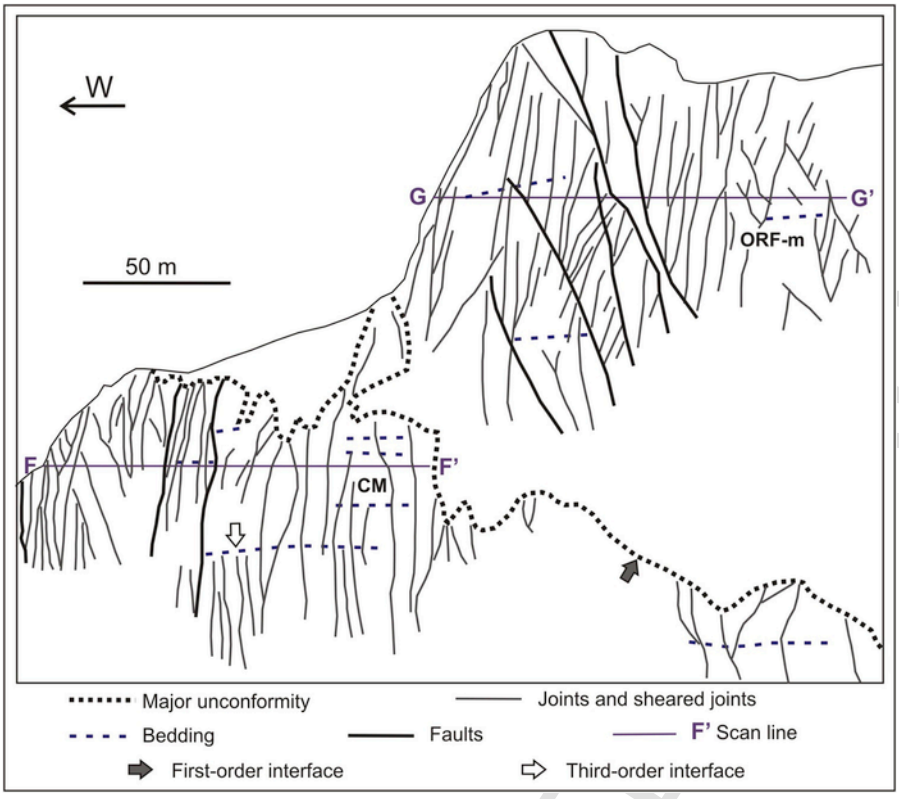

Fig. 10. Cross-sectional drawing from mapping of both stratigraphic and structural elements on the photo of Fig. 4b. Areas lacking such elements are covered by vegetation and/or recent slope debris. CM = Cima delle Murelle Formation (grainstone-dominated facies association); ORF-m = Orfento Formation (massive facies association).

plied remote stress state and/or material rotation (Wilkins et al., 2001; Myers and Aydin, 2004). In addition, joints and veins perpendicular to bedding formed at a very early stage (shallow burial depth) prior to Maiella anticline development (Lavenu et al., 2014), and could therefore be reactivated during the Maiella folding. No clear evidence is found in the carbonate succession for the presence of bed-perpendicular pressure solution seams that, according to several authors (Graham-Wall et al., 2003; Antonellini et al., 2008; Agosta et al., 2009; Aydin et al., 2010), formed during the initial stages of Maiella folding and were reactivated through flexural slip. However, their original occurrence is not excluded as many fractures have been weathered and enlarged by recent dissolution;

(ii) progressive fracture and fault linkage through slip episodes along their planes, similar to those documented in Maiella by Antonellini et al. (2008) and Agosta et al. (2009). Undulations (jogs and steps) along some fault planes and VPF (Figs. 8–11) record this process.

6. Fracture stratigraphy

The different spacing distributions displayed by the graph in Fig. 13 suggest a stratigraphic and lithologic control on fracture spacing and likely on other fracture characteristics. Based upon substantial difference in fracture spacing, heights and geometry, the studied carbonate succession is subdivided into three major fracture units (Fig. 1c): (i) Cima delle Murelle Formation, (ii) massive facies association of the Orfento Formation and (iii) cross-bedded facies association of the Orfento Formation (Figs. 8–10). The grainstone-dominated facies association of the Cima delle Murelle Formation presents fractures with characteristics similar to those occurring within the underlying micrite-dominated facies association of the same formation (Stefano Torrieri, 2012, personal communication). For this reason, the entire Cima delle Murelle Formation is considered as a single major fracture unit. Smaller-scale (meters to a few tens of meters thick), minor fracture units (Fig. 1c) also occur within both the Cima delle Murelle and the Orfento formations. The well-constrained fracture units composing the former formation are discussed in this section.

Based upon abutting and crosscutting relationships among fractures and stratigraphic surfaces (i.e., FTI concept) of different-rank: boundaries of different formations, facies associations and facies, respectively, a three-fold hierarchy of interfaces is proposed (see Fig. 1c for the hierarchical concept of interface; a concept recently used also by Panza et al., 2016). In the proposed hierarchy, interfaces are not weak rock veneers as reported in some literature (e.g., Underwood et al., 2003; Cooke et al., 2006). As shown along the northern and southern walls of the surveyed gorge (Figs. 4, 8 and 10), the unconformable boundary between the Orfento and the Cima delle Murelle formations represents a first-order interface (Fig. 14; FTI > 90%, estimated from Fig. 9). In fact, swarms of fractures up to 150 m high and possibly more, forming the widest fault damage zones cutting across the Cima delle Murelle Formation, abruptly terminate upward against this interface (Figs. 8 and 10). No difference is noticed whether the interface juxtaposes the Cima delle Murelle Formation with either the grainstones or the discontinuous layer of channel lag breccias of the Orfento Formation (Fig. 9).

A second-order interface is represented by the boundary between the two facies associations (major fracture units) of the Orfento Formation, in which most of the up to 70 m high fractures crosscutting its massive facies association seem to terminate (FTI between 60 and 70% estimated from Fig. 8).

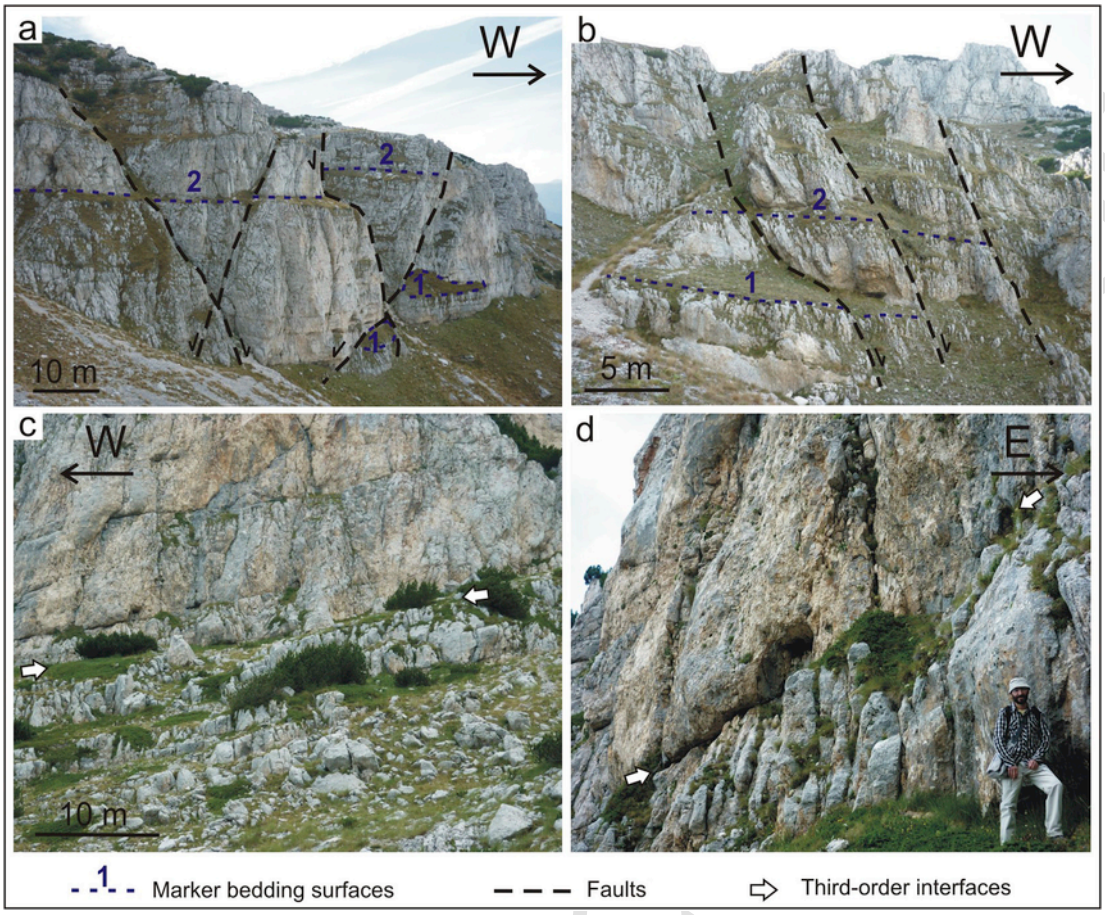

Fig. 11. Outcrop views of fault zones within the grainstone-dominated facies association of the Cima delle Murelle Formation. a–b) Fault zones of which fault planes are highlighted by dashed lines. The marker bedding surfaces highlight the normal throws of the faults. In (a) NNW-striking faults dislocate earlier ENE-striking faults. c–d) Third-order interfaces separating rudist floatstone banks, some meters thick, from the underlying thinner beds varying in facies, which are more densely fractured (surveyed sites H and I, cf. Fig. 3 and 4b). The geologist is for scale.

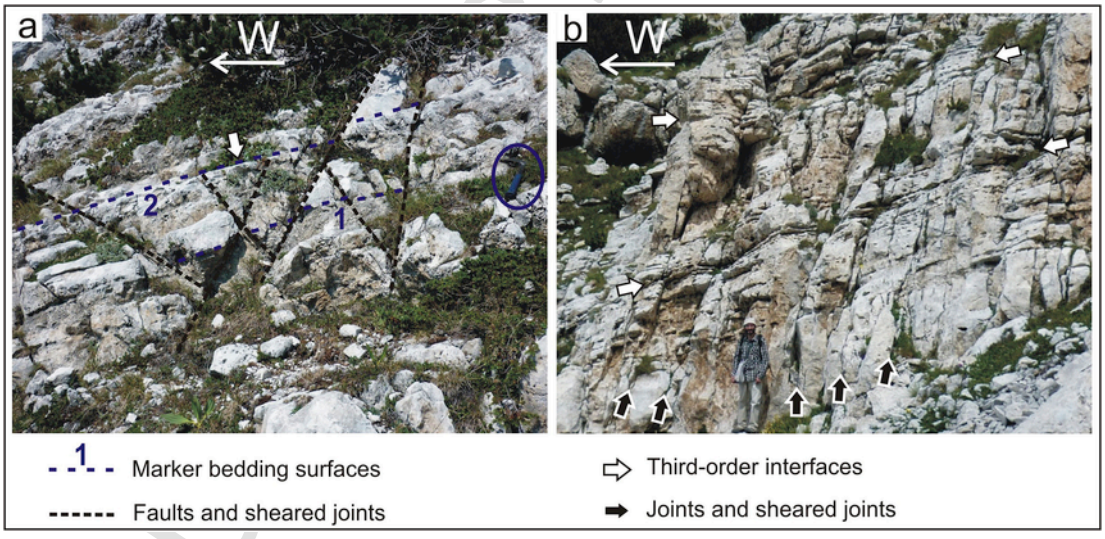

Fig. 12. Outcrop views of faults, joints and sheared joints within the Orfento Formation. a) Fracture network made up of oblique-to-bedding incipient faults and sheared joints present within the massive facies association (surveyed site L, cf. Fig. 3 and 4b). The marker bedding surfaces highlight the normal throws of the faults. The 33-cm long hammer is for scale. b) Near-parallel joints and sheared joints forming a fault damage zone within the cross-bedded facies association (surveyed site N, cf. Fig. 3). These joints abut against well-defined bed surfaces (third-order interfaces). The geologist is for scale.

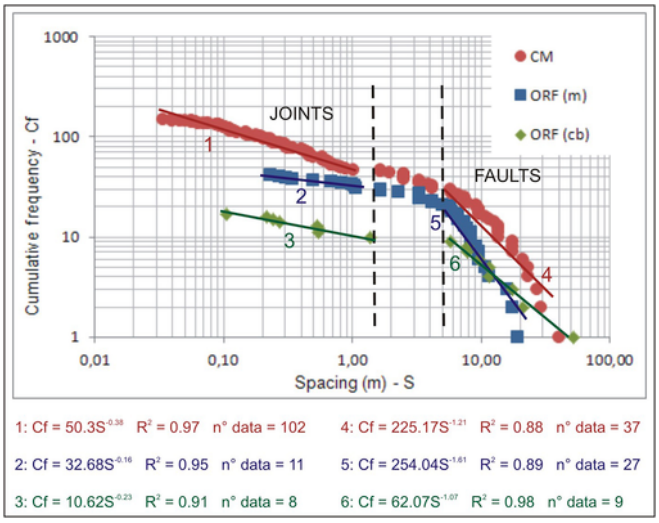

Fig. 13. Cumulative frequency distributions of spacing computed for analyzed fractures: joints and faults. The best-fit power law correlations of the data points are displayed. CM = Cima delle Murelle Formation (grainstone-dominated facies association); ORF (m) = Orfento Formation (massive facies association); ORF (cb) = Orfento Formation, (cross-bedded facies association).

Third-order interfaces are recognized within both the Cima delle Murelle and Orfento formations. In the former formation, the interfaces are generally represented by the sharp boundaries of the over 2 m thick rudist floatstone banks (Fig. 11c–d, 14). Although generally unable to stop the major fault planes and the highest damage zone fractures, such interfaces stop some meters to a few tens of meters high fractures (FTI between 30 and 80% estimated from Figs. 8, 10 and 11) cutting across packages of beds that, although varying in facies (including also rudist floatstone beds), attain individual thickness typically less than 2 m (mostly decimeters). The over 2 m thick rudist floatstone banks, which are less densely fractured than the aforementioned multi-facies bed packages (60 cm versus 26 cm of mean fracture spacing, calculated from field-measured data of Table 2), represent well-constrained small-scale (minor) fracture units within the Cima delle Murelle Formation. The susceptibility of rudist-bearing banks to fracturing as distinct fracture units within relatively thinner-bedded and more densely fractured carbonate successions was already documented in literature (Cooke et al., 2006; Di Cuia et al., 2009).

In the cross-bedded facies association of the Orfento Formation, up to 20 m high fractures forming the fault damage zones terminate against some laterally extensive sharp bed surfaces. These surfaces separate various facies and display a negative relief due to erosion, and karstic dissolution features localized preferentially along them (Figs. 8, 12b and 14). Such bed surfaces thus represent third-order interfaces (FTI ranging from 50 to 90%, estimated from Figs. 8 and 12b). Thin section observations revealed that near these sharp bed surfaces grainstones are more intensely burrowed than elsewhere. Since intense burrowing typically indicates low sedimentation rates (Flügel, 2004), sharp bed surfaces are interpreted as the result of relatively long-lived periods of non-deposition on the seafloor.

Within the massive facies association of the Orfento Formation, the third order interfaces (relatively well-defined bed surfaces with FTI not exceeding 20–30%) are much rarer than in the previous one, due to ubiquitous bed amalgamation that produced ill-defined bed surfaces (Figs. 9 and 12a). Boundaries of breccia layers represent additional third-order interfaces, against which a few tens of meters high fractures terminate (Fig. 9).

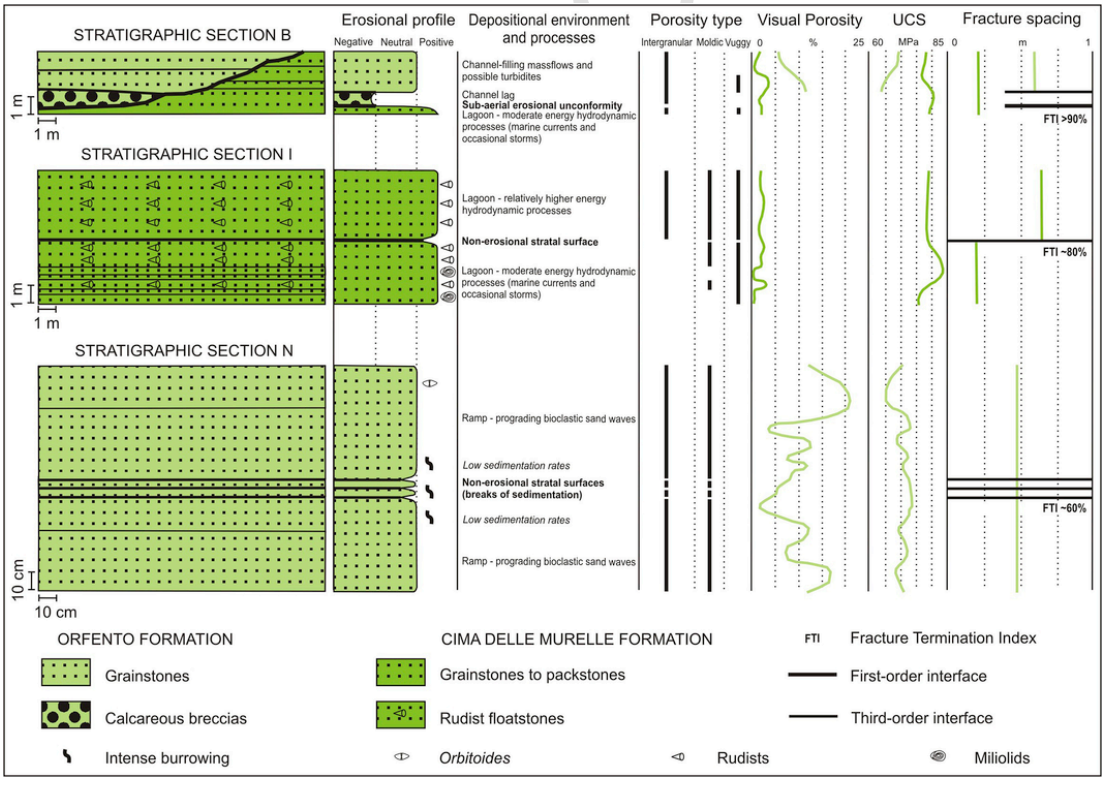

Fig. 14. Stratigraphic logs across the best exposed fracture unit interfaces of the study area.

To sum up, first- and second-order interfaces bounding major and thicker fracture units were able to arrest higher fault-related fractures than smaller-scale third-order interfaces bounding minor fracture units, in agreement with the outcomes of Wilkins and Gross (2002).

7. Lithologic control on fracture characteristics

Based upon qualitative thin section observations, quantitative data (Tables 1 and 2) and correlation graphs (Fig. 15), the lithologic control on the characteristic of the studied fractures is unraveled. It is well known that the mechanical properties of a rock can be represented by Uniaxial Compressive Strength (UCS), which exerts a control on fracturing (Corbet et al., 1987; Bai and Pollard, 2000; Lezin et al., 2009; Rustichelli et al., 2013a; Lavenu et al., 2014; Michie et al., 2014). Commonly, stiffer rocks (high UCS values) generate denser fracture networks relative to softer rocks undergoing failure. Accordingly, the Orfento Formation (UCS = 63.5–73.5 MPa) as a whole displays a lower fracture density and higher spacing values (Figs. 8, 9 and 13) than the Cima delle Murelle Formation (UCS = 65–84.5 MPa). By contrast, the cross-bedded facies association of the Orfento Formation (UCS = 67–73.5 MPa) shows a lower fracture density and higher fracture spacing values (Figs. 8 and 13) than the massive facies association (UCS = 63.5–70 MPa). This may be due to a bias on Schmidt Hammer testing but also to the fact that the UCS of the rock measured in outcrop may be different from that at the time of fracture formation, due to later diagenetic modifications (Shackleton et al., 2005; Laubach et al., 2009).

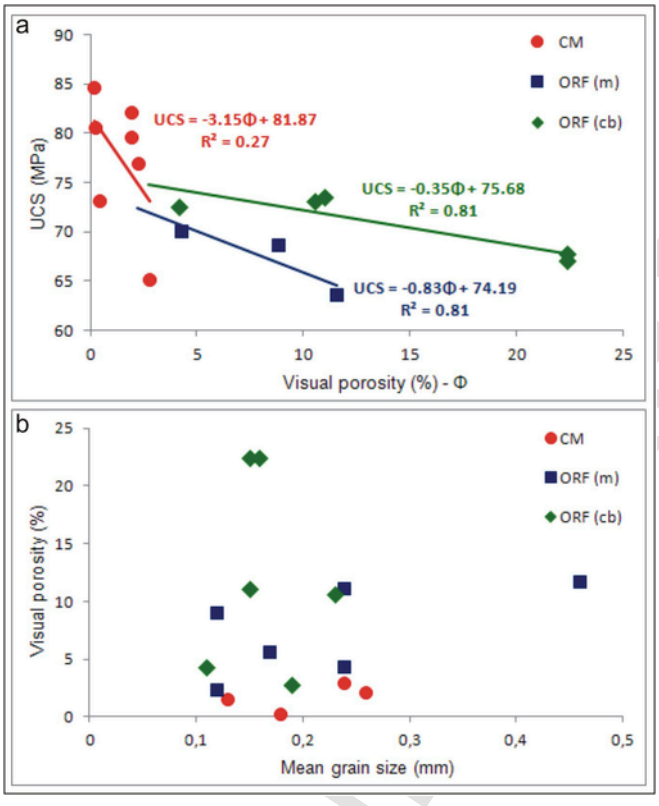

Fig. 15. Correlation graphs among some intrinsic rock parameters of the studied carbonate rocks. Each data point represents the mean values of the cross-plotted parameters computed for each sample (see Table 1). a) The graph shows the best-fit linear correlations between visual porosity and UCS. b) The graph shows that mean grain size is not correlated to the visual porosity. CM = Cima delle Murelle Formation (grainstone-dominated facies association); ORF (m) = Orfento Formation (massive facies association); ORF (cb) = Orfento Formation, (cross-bedded facies association).

In agreement with published literature (Corbet et al., 1987; Lezin et al., 2009; Rustichelli et al., 2013a) that found negative correlations between UCS and total rock porosity, good negative correlations are shown in Fig. 15a between UCS and visual porosity of the Orfento Formation, whereas a poor negative correlation characterizes the Cima delle Murelle Formation. Although likely ignoring some microporosity, we consider visual porosity as the porosity measurement that can better approximate the total rock porosity with respect to the connected porosity. This is especially true in the Orfento Formation, where a major part of porosity is not connected.

In contrast with previous works on carbonates worldwide (e.g., Hanks et al., 1997; Lucia, 1999; Ehrenberg and Nadeau, 2005; Wennberg et al., 2006; Rustichelli et al., 2012, 2013a,b), both qualitative thin section observations (Fig. 6) and quantitative data indicate that visual porosity of the studied rocks is poorly dependent on rock texture, mean grain size, grain sorting and grain shape. Indeed, packstones, grainstones, floatstones and rudstones of the Cima delle Murelle Formation have similar low values of visual porosity (0–3%; Table 1), whereas grainstones of the Orfento Formation display a broader range of visual porosity values (~2–22%), which are not proportional to the mean grain size (Fig. 15b).

On the contrary, lower values of visual porosity of the Cima delle Murelle Formation relative to the Orfento Formation are mainly due to the abundant (up to 30% vol of the whole rock) intergranular void-filling calcite cement and eventual presence of matrix (up to 25% vol), which in contrast are minimal (from <1% to a few units % vol) and absent within the Orfento Formation, respectively (Fig. 6).

Physical compaction grade (qualitative grain packing estimation on thin sections), due to overburden, reached by the rocks belonging to Orfento Formation is considered the major factor responsible for its broad visual porosity range (Fig. 6e–f). Although cement is rare in all the facies of this formation, a minimal additional amount (<1%) of early, pre-compactional cement able to fairly join together the grains, may have made the difference in preventing physical compaction, and hence intergranular (mainly) and moldic porosity loss, in the present-day most porous facies (Fig. 6f). A similar explanation for intergranular porosity preservation was provided by Ronchi et al. (2010). In agreement with the recent literature (La Croix et al., 2013 and references therein), burrowing is another factor to be taken into account for such a remarkable visual porosity difference among the various facies. This biogenic process had a dual role in influencing either porosity gain or loss, facies by facies, according to burrow types and host rock porosity. In particular, due to localized, early physical compaction (with commonly associated early cementation) around some types of burrows (Fig. 6g), a certain amount of porosity (a few units % vol of the whole rock) due to the burrowing itself is generally preserved as well within facies that underwent the highest overburden-related physical compaction.

To sum up, this study reveals that substantial differences in spacing and distribution of VPF in distinct carbonate rock types can be due to different mechanical properties and porosity values, which in turn are a result of variations in depositional settings and biogenic, sedimentologic and diagenetic processes, as similarly reported by Rustichelli et al. (2013a, 2015) for stratabound fractures.

8. Fluid flow properties of fractured platform and ramp carbonates

In this section, data on fracture geometry, connectivity, and dimensional parameters documented for the VPF networks within the

Cima delle Murelle Formation (Bahamian-type inner platform carbonates) and the overlaying Orfento Formation (proximal ramp carbonates) are discussed in terms of both vertical and horizontal permeability within the carbonate multilayer (Fig. 16).

The platform carbonates represent a tight major fracture unit that is largely crosscut by high-angle fault zones up to over 100 m high and arranged as approximately orthogonal sets showing cross-cutting relationships. Hence, these fault zones form quite pervasive networks of closely and regularly spaced and well-connected open fractures that can be considered as widespread and efficient pathways for both vertical and horizontal fluid flow. Fault zones could therefore enhance both recovery of hydrocarbons and their migration from potential intra-platform source rocks. The third-order interfaces within the platform carbonates (i.e., boundaries of rudist floatstone banks), due to their moderate efficiency in stopping fractures and limited lateral extent, are not considered as efficient obstacles for fracture-driven upward hydrocarbon flow. Even the first-order interface localized at the platform-ramp boundary likely does not act as a hydrocarbon seal because it consists of an erosional surface around which low-permeability material is missing. Indeed, such a first-order interface may slow down the upward flow of hydrocarbons, which may invade the immediately overlying porous ramp carbonates. Thus, in this model, a potential ramp reservoir could be efficiently charged from the fractured platform carbonates below.

As a whole, the ramp carbonates consist of alternating beds characterized by a pronounced variation of matrix porosity (~2–22%, ~10% on average), which is mostly (~58%) non-connected (non-effective). The studied ramp carbonates may therefore represent a surface analog of a complex reservoir unit of overall fair-poor quality (Levorsen, 1967), in which layers acting as small-scale reservoirs (connected porosity ranging from 5% to 8%) are separated from each other by others acting as baffles or seals (connected porosity < 5%). Due to lack of high-efficiency internal (third-order) interfaces, the massive facies association of the ramp carbonates (Orfento Formation) represents a major fracture unit that, in places, is entirely cross-cut by well-connected networks of VPF. Where present in a subsurface analog stratigraphic unit, such VPF networks could form local but efficient pathways for upward hydrocarbon flow throughout the entire stratigraphic thickness. In contrast, due to presence of more efficient third-order interfaces, VPF affecting the cross-bedded facies association of the ramp carbonates are much shorter (maximum 20 m high) than those within the other studied carbonate units. As these fractures are also relatively widely spaced and poorly connected both vertically and horizontally, they are envisioned as much less efficient pathways for both vertical and lateral hydrocarbon flow within the cross-bedded facies association, so few hydrocarbons escape for potential recovery. However, this increases the probability that hydrocarbons may be stored in ramp carbonate beds characterized by the highest amounts of connected matrix porosity and alternating with low-porosity ones.

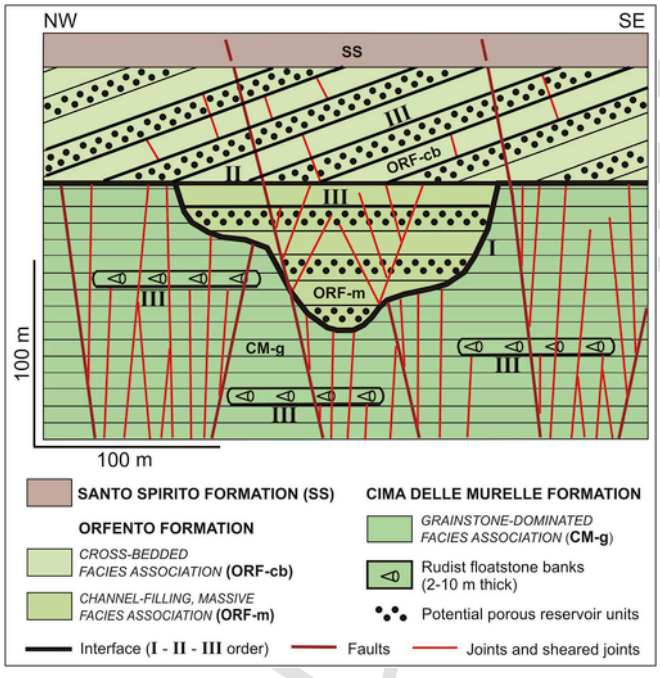

Fig. 16. 2D conceptual model illustrating the characteristics of vertically persistent fractures (VPF) in the studied Cretaceous platform and ramp carbonates. Dip angle of cross-beds is exaggerated and fracture spacing is arbitrary (only the major fractures are resolvable in the scheme). Fault normal throws are not resolvable in the scheme, as these are generally less than 1 m.

9. Conclusions

We present the results of a work aimed at characterizing the vertically persistent fracture (VPF) networks affecting Bahamian-type inner platform carbonates and overlaying proximal ramp carbonates, both Cretaceous in age, which crop out extensively along the Rava del Ferro gorge, Maiella Mountain (central Italy). This field- and laboratory-based work combines both sedimentologic and structural investigations.

The main results are consistent with the following statements:

(i) platform and ramp carbonates are affected by high-angle, oblique-slip normal fault zones striking either NNW-SSE or WSW-ENE. Faults are likely associated with the development of the Maiella anticline, which occurred in Pliocene times. Fault damage zones are from tens to a few hundreds of meters wide and commonly overlapped. These consist of swarms of high-angle to vertical VPF (joints and sheared joints) that are from ~2 m to over 100 m high. In platform carbonates fault damage zones are wider and composed of better connected, higher and less spaced fractures than in the ramp carbonates;

(ii) a three-fold hierarchy of fracture unit interfaces control the fracture distribution in both platform and ramp carbonates. The boundary between the platform and the ramp carbonates represents the most efficient interface; in fact, over 90% of hundreds of meters high fractures forming the largest fault zones crosscutting the platform carbonates, terminate upward against this interface;

(iii) higher fracture density in the platform carbonates with respect to the ramp ones is because the platform carbonates are made up of overall stiffer (higher UCS values) and less porous rocks, due to more abundant intergranular void-filling cement and presence of matrix;

(iv) the well-connected network of closely spaced VPF cutting across the platform carbonates may form efficient pathways for both vertical and horizontal hydrocarbon flow in the subsurface. In contrast, the overall low-density and less connected VPF network affecting the ramp carbonates may prevent the hydrocarbons from escaping upwards and laterally. At the same time, it increases the probability that oil and gas may be stored in ramp carbonate beds characterized by the highest amounts of connected porosity and alternating with low-porosity ones.

Considering the impact that VPF may have on subsurface fluid flow, the acquired knowledge can help the management of hydrocarbon recovery as well as the overall prediction of carbonate reservoir quality.

Acknowledgements

We thank the personnel of Shell Italia E&P for the full support during all work phases. In particular, we acknowledge Elena Manzo for the help provided during the field work, Maurizio Giorgioni and Carlos Pirmez for their useful comments and suggestions. We are grateful to Hannah Riegel for improvements in English language. We also thank the Editor Willem Langenberg and two anonymous reviewers for the improvement of the submitted article, and Michael Sweet, Peter Eichhubl, Stephen Laubach and Scott Wilkins for the constructive reviews of an earlier version. This study has been supported by the Reservoir Characterization Project (www.rechproject.com) and the FAR Project 2014 "Characterization and modelling of natural reservoirs of geofluids in fractured carbonate rocks", funded by the University of Camerino.

References

Accarie, H., Beaudoin, B., Cussey, R., Joseph, P., Triboulet, S., 1986. Dynamique sédimentaire et structurale au passage plate-forme/bassin. Les faciès carbonates Cretacés du massif de la Maiella (Abruzzes, Italie). Mem. Soc. Geol. Ital. 36, 217–231.

Agosta, F., Alessandroni, M., Tondi, E., Aydin, A., 2009. Oblique normal faulting along the northern edge of the Majella anticline, central Italy: inferences on hydrocarbon migration and accumulation. J. Struct. Geol. 31, 674–690.

Agosta, F., Alessandroni, M., Antonellini, M., Tondi, E., Giorgioni, M., 2010. From fractures to flow: a field-based quantitative analysis of an outcropping carbonate reservoir. Tectonophysics 490, 197–213.

Antonellini, M., Tondi, E., Agosta, F., Aydin, A., Cello, G., 2008. Failure modes in deep-water carbonates and their impact for fault development: Majella Mountain, Central Apennines, Italy. Mar. Pet. Geol. 25, 1074–1096.

Aydin, A., 2000. Fractures, faults, and hydrocarbon entrapment, migration and flow. Mar. Pet. Geol. 17, 797–814.

Aydin, A., Antonellini, M., Tondi, E., Agosta, F., 2010. Deformation along the leading edge of the Majella thrust sheet in central Italy. J. Struct. Geol. 32, 1291–1304.

Bai, T., Pollard, D.D., 2000. Fracture spacing in layered rocks: a new explanation based on the stress transition. J. Struct. Geol. 22, 43–57.

Bigi, G., Cosentino, D., Parotto, M., Sartori, R., Scandone, P., 1992. Structural Model of Italy, Scale 1:500,000, 6 Sheets. vol. 114. CNR, Quaderni di Ricerca Scientifica.

Casabianca, D., Bosence, D., Beckett, D., 2002. Reservoir potential of Cretaceous platform-margin breccias, central Italian Apennines. J. Pet. Geol. 25 (2), 179–202.

Chilingarian, G., Mazzullo, S.J., Rieke, H.H., 1996. Carbonate Reservoir Characterization: a Geological-engineering Analysis, Part II. Development in Petroleum Science. . 994 p.

Choquette, P.W., Pray, L.C., 1970. Geologic nomenclature and classification of porosity in sedimentary carbonates. AAPG Bull. 54 (2), 207–244.

Cooke, M.L., Simo, J.A., Underwood, C.A., Rijken, P., 2006. Mechanical stratigraphic controls on fracture patterns within carbonates and implications for groundwater flow. Sediment. Geol. 184 (3–4), 225–239.

Corbet, K., Friedman, M., Spang, J., 1987. Fracture development and mechanical stratigraphy of Austin Chalk, Texas. AAPG Bull. 71 (1), 17–28.

Crescenti, U., Crostella, A., Donzelli, G., Raffi, G., 1969. Stratigrafia della serie calcarea dal Lias al Miocene nella regione marchigiano-abruzzese. Mem. Soc. Geol. Ital. 8, 343–420.

Di Cuia, R., Shakerley, A., Masini, M., Casabianca, D., 2009. Integrating outcrop data at different scales to describe fractured carbonate reservoirs: example of the Maiella carbonates, Italy. First Break 27, 11–21.

Dunham, R.J., 1962. Classification of carbonate rocks according to depositional texture. In: Ham, W.E. (Ed.), Classification of Carbonate Rocks. AAPG Memoir 1. pp. 108–121.

Eberli, G.P., Bernoulli, D., Sanders, D.G.K., Vecsei, A., 1993. From aggradation to progradation: the Maiella platform (Abruzzi, Italy). In: Simo, T., Scott, R.W., Masse, J.P. (Eds.), Atlas of Cretaceous Carbonate Platforms. AAPG Memoir 56. pp. 213–232.

Ehrenberg, S.N., Nadeau, P.H., 2005. Sandstone versus carbonate petroleum reservoirs: a global perspective on porosity-depth and porosity-permeability relationships. AAPG Bull. 89 (4), 435–445.

Embry, A.F., Klovan, J.E., 1971. A late Devonian reef tract on northeastern Banks Island, N. W. T.. Bull. Can. Pet. Geol. 19 (4), 730–781.

English, J.M., 2012. Thermomechanical origin of regional fracture systems. AAPG Bull. 96, 1597–1625.

Flügel, E., 2004. Microfacies of Carbonate Rocks: Analysis, Interpretation and Application. Springer-Verlag, Berlin, Heidelberg, New York. 976 p.

Garland, J., Neilson, J.E., Laubach, S.E., Whidden, K.J., 2012. Advances in carbonate exploration and reservoir analysis. In: Garland, J., Neilson, J.E., Laubach, S.E., Whidden, K.J. (Eds.), Advances in Carbonate Exploration and Reservoir Analysis. Geological Society of London, Special Publication 370, pp. 1–15.

Ghisetti, F., Vezzani, L., 2002. Normal faulting, extension and uplift in the outer thrust belt of the central Apennines (Italy): role of the Caramanico fault. Basin Res. 14, 225–236.

Gillespie, P.A., Howard, C.B., Walsh, J.J., Watterson, J., 1993. Measurement and characterization of spatial distribution of fractures. Tectonophysics 226, 113–141.

Graham-Wall, B., Antonellini, M., Aydin, A., 2003. Formation and growth of normal faults in carbonates within a compressive environment. Geology 31, 11–14.

Graham-Wall, B., Girgacea, R., Mesonjesi, A., Aydin, A., 2006. Evolution of fluid pathways through fracture controlled faults in carbonates of the Albanides fold-thrust belt. AAPG Bull. 90, 1227–1249.

Hanks, C.L., Lorenz, J.C., Teufel, L., Krumhardt, A.P., 1997. Lithology and structural controls on natural fracture distribution and behavior within the Lisburn group, northeastern Brooks Range and North Slope subsurface, Alaska. AAPG Bull. 81, 1700–1720.

Hooker, J.N., Laubach, S.E., Marrett, R., 2013. Fracture-aperture size–frequency, spatial distribution, and growth processes in strata-bounded and non-strata-bounded fractures, Cambrian Mesón Group, NW Argentina. J. Struct. Geol. 54, 54–71.

Jacquemyn, C., Swennen, R., Ronchi, P., 2012. Mechanical stratigraphy and (palaeo-) karstification of the Murge area (Apulia, southern Italy). In: Garland, J., Neilson, J.E., Laubach, S.E., Whidden, K.J. (Eds.), Advances in Carbonate Exploration and Reservoir Analysis. Geological Society of London, Special Publications 370, pp. 169–186.

La Croix, A.D., Gingras, M.K., Pemberton, S.G., Mendoza, C.A., MacEachern, J.A., Lemiski, R.T., 2013. Biogenically enhanced reservoir properties in the Medicine Hat gas field, Alberta, Canada. Mar. Pet. Geol. 43, 464–477.

Laubach, S.E., 2003. Practical approaches to identifying sealed and open fractures. AAPG Bull. 87, 561–579.

Laubach, S.E., Olson, J.E., Gross, M.R., 2009. Mechanical and fracture stratigraphy. AAPG Bull. 93 (11), 1413–1426.

Lavenu, A.P.C., Lamarche, J., Salardon, R., Gallois, A., Mariè, L., Gauthier, B.D.M., 2014. Relating background fractures to diagenesis and rock physical properties in a platform-slope transect. Example of the Maiella Mountain (central Italy). Mar. Pet. Geol. 51, 2–19.

Levorsen, A.H., 1967. Geology of Petroleum. Freeman W.H., San Francisco – London. 724 p.

Lezin, C., Odonne, F., Massonnat, G.J., Escadeillas, G., 2009. Dependence of joint spacing on rock properties in carbonate strata. AAPG Bull. 93 (2), 271–290.

Lucia, F.J., 1999. Carbonate Reservoir Characterization. Springer-Verlag, New York. 226 p.

Marchegiani, L., Van Dijk, J.P., Gillespie, P.A., Tondi, E., Cello, G., 2006. Scaling properties of the dimensional and spatial characteristics of fault and fracture systems in the Majella Mountain, central Italy. In: Cello, G., Malamud, B. (Eds.), Fractal Analysis for Natural Hazards. Geological Society of London, Special Publication 261, pp. 113–131.

Masini, M., Bigi, S., Poblet, J., Bulnes, M., Di Cuia, R., Casabianca, D., 2011. Kinematic evolution and strain simulation, based on cross-section restoration, of the Maiella Mountain: an analogue for oil fields in the Apennines (Italy). In: Poblet, J., Lisle, R.J. (Eds.), Kinematic Evolution and Structural Styles of Fold-and-thrust Belts. Geological Society of London, Special Publication 349, pp. 25–44.

Michie, E.A.H., Haines, T.J., Healy, D., Neilson, J.E., Timms, N.E., Wibberley, C.A.J., 2014. Influence of carbonate facies on fault zone architecture. J. Struct. Geol. 65, 82–99.

Mutti, M., 1995. Porosity Development and Diagenesis in the Orfento Supersequence and its Bounding Unconformities (Upper Cretaceous, Montagna Della Majella, Italy). AAPG, Special Publication 63, 141–158.

Mutti, M., Bernoulli, D., Eberli, G.P., Vecsei, A., 1996. Depositional geometries and facies associations in an upper Cretaceous prograding carbonate platform margin (Orfento supersequence, Maiella, Italy). J. Sediment. Res. 66 (4), 749–765.

Myers, R., Aydin, A., 2004. The evolution of faults formed by shearing across joint zones in sandstones. J. Struct. Geol. 26, 947–966.
Odling, N.E., Gillespie, P., Bourgine, B., Castaing, C., Chiles, J.P., Christensen, N.P., Fillion, E., Genter, A., Olsen, C., Thrane, L., Trice, R., Aarseth, E., Walsh, J.J., Watterson, J., 1999. Variations in fracture system geometry and their implications for fluid flow in fractured hydrocarbon reservoirs. Pet. Geosci. 5, 373–384.
Panza, E., Agosta, F., Zambrano, M., Tondi, E., Prosser, G., Giorgioni, M., Janiseck, J.M., 2015. Structural architecture and Discrete Fracture Network modelling of layered fractured carbonates (Altamura Fm., Italy). Ital. J. Geosci. 134 (3), 409–422. Special Issue on "Fractured carbonate reservoirs and fluid flow".
Panza, E., Agosta, F., Rustichelli, A., Zambrano, M., Tondi, E., Prosser, G., Giorgioni, M., Janiseck, J.M., 2016. Fracture stratigraphy and fluid flow properties of shallow-water, tight carbonates: the case study of the Murge Plateau (southern Italy). Mar. Pet. Geol. 73, 350–370.
Pizzi, A., Falcucci, E., Gori, S., Galadini, F., Messina, P., Di Vincenzo, M., Esestime, P., Giaccio, B., Sposato, A., 2010. Active faulting in the Maiella massif (Central Apennines, Italy). Geoacta 57–73. Special Publication 3.
Pollard, D.D., Aydin, A., 1988. Progress in understanding jointing over the past century. Geol. Soc. Am. Bull. 100, 1181–1204.
Price, N.J., Cosgrove, J.W., 1990. Analysis of Geological Structures. Cambridge University Press, New York. 520 p.
Ronchi, P., Ortenzi, A., Borromeo, O., Claps, M., Zempolich, W.G., 2010. Depositional setting and diagenetic processes and their impact on the reservoir quality in the late Visean–Bashkirian Kashagan carbonate platform (Pre-Caspian Basin, Kazakhstan). AAPG Bull. 94 (9), 1313–1348.
Rustichelli, A., Tondi, E., Agosta, F., Cilona, A., Giorgioni, M., 2012. Development and distribution of bed-parallel compaction bands and pressure solution seams in carbonates (Bolognano Formation, Majella Mountain, Italy). J. Struct. Geol. 37, 181–199.
Rustichelli, A., Agosta, F., Tondi, E., Spina, V., 2013a. Spacing and distribution of bed-perpendicular joints throughout layered, shallow-marine carbonates (Granada Basin, southern Spain). Tectonophysics 582, 188–204.
Rustichelli, A., Tondi, E., Agosta, F., Di Celma, C., Giorgioni, M., 2013b. Sedimentologic and diagenetic controls on pore-network characteristics of Oligocene-Miocene ramp carbonates (Majella Mountain, central Italy). AAPG Bull. 97 (3), 487–524.
Rustichelli, A., Iannace, A., Girundo, M., 2015. Dolomitization impact on fracture density in pelagic carbonates: contrasting case studies from the Gargano Promontory and the Southern Apennines (Italy). Ital. J. Geosci. 134 (3), 556–575. Special Issue on "Fractured carbonate reservoirs and fluid flow".
Scisciani, V., Tavarnelli, E., Calamita, F., 2002. The interaction of extensional and contractional deformation in the outer zones of the Central Apennines, Italy. J. Struct. Geol. 24, 1647–1658.
Shackleton, J.R., Cooke, M.L., Sussman, A.J., 2005. Evidence for temporally changing mechanical stratigraphy and effects on joint-network architecture. Geology 33, 101–104.
Solano, N., Zambrano, L., Aguilera, R., 2011. Cumulative-gas-production distribution on the Nikanassin Formation, Alberta and British Columbia, Canada. SPE Reserv. Eval. Eng. 14, 357–376.
Stearns, D.W., 1968. Certain aspect of fracture in naturally deformed rocks. In: Rieker, R.E. (Ed.), National Science Foundation Advanced Science Seminar in Rock Mechanics: Special Report. Air Force Cambridge Research Laboratories, Bedford, Massachusetts, pp. 97–118.
Terzaghi, R., 1965. Sources of error in joint surveys. Geotechnique 15, 287–304.
Tondi, E., Antonellini, M., Aydin, A., Marchegiani, L., Cello, G., 2006. The role of deformation bands and pressure solution seams in fault development in carbonate grainstones of the Majella Mountain, Italy. J. Struct. Geol. 28, 376–391.
Tucker, M.E., Wright, V.P., 1990. Carbonate Sedimentology. Oxford, Blackwell. 482 p.
Underwood, C.A., Cooke, M.L., Simo, J.A., Muldoon, M.A., 2003. Stratigraphic controls on vertical fracture patterns in Silurian dolomite, northeastern Wisconsin. AAPG Bull. 87, 121–142.
Vecsei, A., 1991. Aggradation un Progradation eines karbonatplatform-Randes: Kreide bis Mittleres Tertiär der Montagna della Maiella. Mitteilungen aus dem Geologischen Institut der Eidgenössischen Technischen Hochschule und der Universitat Zürich, Abruzzen. Neue Folge 294.
Vecsei, A., Sanders, D.K., Bernoulli, D., Eberli, G.P., Pignatti, J.S., 1998. Cretaceous to Miocene Sequence Stratigraphy and Evolution of the Maiella Carbonate Platform Margins, Italy. 53–73. SEPM Special Publication 60.
Watterson, J., 1986. Fault dimensions, displacement and growth. Pure Appl. Geophy. 124, 365–373.
Wennberg, O.P., Svånå, T., Azizzadeh, M., Aqrawi, A.M.M., Brockbank, P., Lyslo, K.B., Ogilvie, S., 2006. Fracture intensity vs. mechanical stratigraphy in platform top carbonates: the Aquitanian of the Asmari Formation, Khaviz anticline, Zagros, southwest Iran. Pet. Geosci. 12 (3), 235–246.
Wilkins, S.J., Gross, M.R., Wacker, M., Eyal, Y., Engelder, T., 2001. Faulted joints: kinematics, displacement-length scaling relations and criteria for their identification. J. Struct. Geol. 23, 315–327.
Wilkins, S.J., Gross, M.R., 2002. Normal fault growth in layered rocks at Split Mountain, Utah: influence of mechanical stratigraphy on dip linkage, fault restriction and fault scaling. J. Struct. Geol. 24, 1413–1429.